NTNU

Norwegian University of
Science and Technology

Multi-frequency backscattering from the sea floor; can the frequency response be used to identify typical sandeel grounds?

Martin Baisgård

Master of Science in Electronics
Submission date: June 2008
Supervisor: Hefeng Dong, IET

Norwegian University of Science and Technology
Department of Electronics and Telecommunications

Problem Description

Find a difference between substrates that usually contain tobis from substrates that do not contain tobis. Give a detailed description of how the backscattering from the sea floor can be processed. Based on this description, look at the differences between four frequencies. Evaluate the disciminating power of features in bottom echoes for the frequencies.

Assignment given: 04. February 2008
Supervisor: Hefeng Dong, IET

Abstract

In this report a phenomenological characterization technique of received bottom echoes has been developed and studied, to evaluate the potential of locating typical sandeel grounds. Data from a calibrated multi–frequency echosounder collected during a **S**urvey **M**ethods for **A**bundance Estimation of **S**andeel (Ammodytes marinus) **S**to**c**ks (SMASSC) survey in the sandeel fishing grounds of "Vestbanken" and "Elbow Spit North", were processed with developed scripts in Matlab to extract first received bottom echo parameters. Together with Simrad SEABEC results and sandeel samples, possible distinctive parameters were found for what could be sandeel grounds. However, ambiguities caused by ping to ping fluctuations and complex behavior of the sandeel species make the characterization difficult. Many of the calculated echo parameters showed possible discrimination power for a future multi–variate analysis.

Preface

I would like to thank the Institute of Marine Research in Bergen for the invitation to the 2008 SMASSC survey in the North Sea and the crew on board S/V Johan Hjort for making the stay an excellent experience. A special thanks goes to Egil Ona at IMR who has been very helpful and my supervisor at NTNU Hefeng Dong.

If there should be any interests of a copy of this report or questions about statements or Matlab scripts, do not hesitate to contact Martin Baisgaard at baisgard@alumni.ntnu.no or by the telephone number (+47) 98452230.

Martin Baisgaard

Contents

1 Introduction

1.1 Motivation

The sandeel is a key–link for the ecosystem especially in the sea, but also on land near the shore. Predators that hunt and eat sandeels are both mammals, fish and birds. In the 1990's the sandeel supported the largest fishery in the North Sea, exceeding one million tonnes. However, the latest years have shown a critical decrease in sandeel biomass in the North Sea, with a landing less than 170 thousand tonnes in 2005 as a minimum. This decrease suggests that the sandeel stock is on the point of depletion in the North Sea. In–depth research to understand and get information on the sandeel is therefore important. To collect the necessary information needed, acoustic surveys of the most important fishing grounds are now being executed. In the Norwegian economical zone, these surveys are first of all carried out by the Institute of Marine Research in Bergen. The main goal of these surveys are to collect enough information, both acoustically and by fish samples, to provide a biomass estimation of the relevant fishing grounds. Also information on the year- and size–classes are collected. The biomass estimation is then used for forming regulations and setting the quotas of the certain grounds.

When finding the estimates of biomass, acoustics are used to both locate and collect information from fish schools of a survey area. By looking at the frequency response of the target strength of a certain school, it is possible to discriminate both type of fish and distribution of fish sizes within the school. The target strength also carries information about the number of fish of the certain size classes. When all information of the schools from the survey are processed, it is combined, and a biomass estimation of the whole survey area can be found statistically.

This way of finding the biomass relies on the fact that *all* fish are located in the water column, when all acoustic data are collected. Therefore the fact that sandeels spend most of their time buried in the sea bed, will give some ambiguity to the biomass results. There is not enough to only rely on the biological fact that most sandeels seek the open seas to feed during daytime and therefore can be estimated by acoustics during this period. If a great quantity still is located in the sea bed, the biomass can be underestimated. Even worse, if it is *thought* that a great quantity still is located in the sea bed, the biomass can be heavily overestimated. If so, a consequence can be unjustifiable overfishing of sandeels.

To reduce the ambiguities and ease the process of a biomass estimation, the sandeel seabed habitats must be located by a fast and reliable technique. There is also important to have the possibility of storing maps of the habitats for later surveys. These can be of great sizes, covering large areas. An approach that may fulfill these specified needs is by exploiting the acoustic properties of the sea floor. A goal for this approach is to use the same acoustic equipment for both fish finding and to classify typical sandeel grounds.

1.2 Introduction to seabed classification

The principle idea behind sea bed classification by acoustics, is based on that different sea floor properties will give different characteristics of the echo received from the sea floor. The received echo shape will be highly dependent upon the properties both close to the sea floor, at the sea floor interface and in the sediment of the sea floor. Some factors affecting the echo shape are illustrated in figure 1.

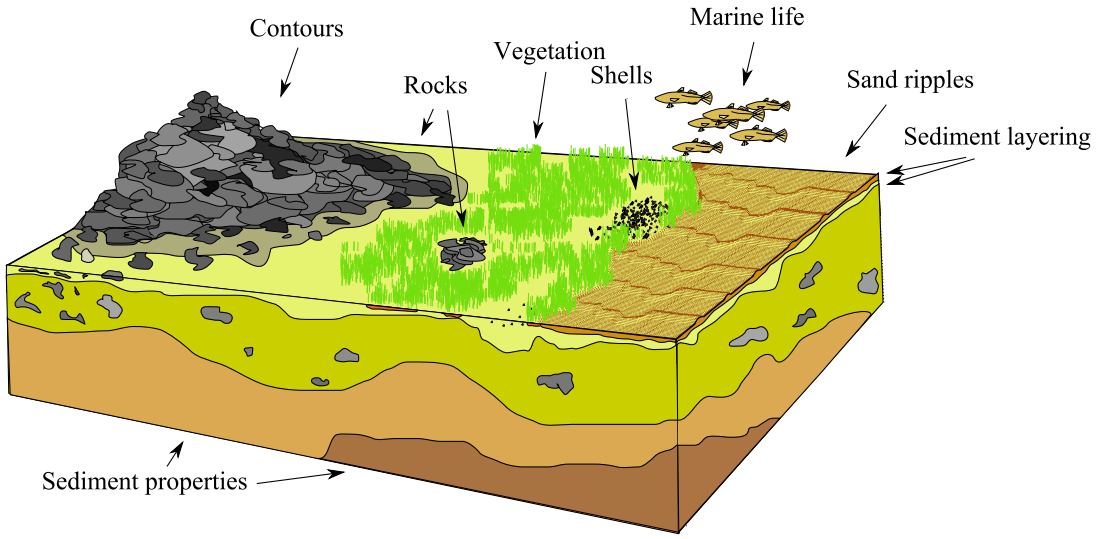

Figure 1

In addition to the properties of the sea floor, the received echo will be highly dependent upon the equipment used for both transmitting and receiving the acoustic signal – and this equipment's different parameters. Some of the most important factors of the equipment that will affect the received echo are

- the frequency; determines the wavelength of the acoustic signal, affects the acoustical signal's penetration properties into the sediment and the signal's sensitivity to roughness of the sea floor. Other environmental factors do also vary with frequency.
- the beam width and beam direction; determines the portion of the echo to be received and the direction of both transmission and receiving. The direction can alter the angle of incident.
- the pulse length; changes the echo pattern.
- the signal strength; will affect the S/N ratio.

1.3 Previously work

In recent years a number of high-frequency ($> 10kHz$) echo analysis techniques have been developed for characterizing the upper layer of seafloor sediments. Typically, these techniques are divided into two separate ways of performing the characterizations.

The first technique is the phenomenological approach, which identify nonparametric measured echo characteristics with core samples or bottom photographs. These systems typical require calibration of signal characteristics of known bottom type and classifications are therefore not absolute. When care is taken, the general experience is that useful classifications can be obtained with these acoustic systems [1]. Two well known commercial systems that use the phenomenological approach are RoxAnn and QTC–View. These two systems analyse the received echoes in slightly different ways, where RoxAnn uses a multi–echo approach while QTC–View a single echo approach. In another word RoxAnn analyses both the first bottom echo reflection and the second reflection, while QTC–View only is analysing the first echo from the sea floor.

The other sediment classification technique is the physical–approached technique. In this technique, sediment characteristics are estimated by comparing measurements to predictions made with physical models. Some advantages with such a technique is that pre–survey calibration requirements are minimized and more detailed sea floor parameters can be found by inversion.

Hamilton emphasizes however that inversion doubtful will allow reliable estimates of bottom type for the complicated and variegated seabed types experienced in the real world [1]. In particular shell components can cause unpredictable returns and particular echo shapes need not have a unique cause.

1.4 Scope and outline

In this report the phenomenological approach will be given main attention for analysing the sea bed. The physical–approached technique will only be used to develop theoretical expressions necessary for understanding the complex behavior of the sea floor echo. Based on the data available, collected by a calibrated Simrad ER500 multi–frequency echosounder during a sandeel assessment survey in the North–Sea, only the first received echo will be used for the sea floor classification. This is due to the available *multi–frequency* echo data, which limits the necessity of a *multi–echo* analyzation – the multiple echoes are mainly used for bottom hardness estimates, which also can be provided by comparing echoes received on different frequency–channels. In addition, it is important to note the lack of information in the frequency spectrum of the received echoes. This is due to a limited bandwidth in most acoustic fish finding equipment. Therefore the frequency spectrum of the received signals have not been analysed in this project. The main focus has been the time–response of the received bottom echoes.

After an introduction to the necessary theory for understanding the behavior of the sea floor echo, the report will give a description of the data acquisition during the sandeel assessment survey. In this section important parameters of the equipment used during the survey are presented and discussed.

A basic approach on processing of echosounder data will follow the data acquisition section. The main focus is to establish processing principles of how to pick the bottom echo, reduce in–stability from ping to ping and at last performing variable calculations of the received echoes. The processing principles are described and discussed with words and illustrations in the report, while script is given on a separate CD as an attachment.

Last, calculated echo variable results will be given for data collected during the survey and processed with the established processing techniques. Different parts of the sea floor will be analysed, based on results provided by the Simrad SEABEC software and sandeel samples from the survey. The main focus is to look for differences between variables calculated for processed bottom echoes at different frequency channels.

2 Theory

2.1 The sandeel (nor. "Tobis")

Sandeels are small eel-like fish, that spend most of their time burrowed in the sea substrate. They burrow themselves into the sediments whenever they are not feeding or mating. In the North Sea, the species lesser sandeel is the most common sandeel.

Figure 2: Picture of a sandeel

During winter, the sandeel hibernate burrowed in the sediments, only coming up from the hiding place for mating around New Year. Around March/April the sandeel emerges from the sea bed at daytime to eat zooplankton, and return to hide during the night. This continues until June/July for older sandeels and until October for younger, when they again burrow themselves into the sediments to hibernate. The sandeel has no swim bladder, which makes it difficult to see with an echosounder.

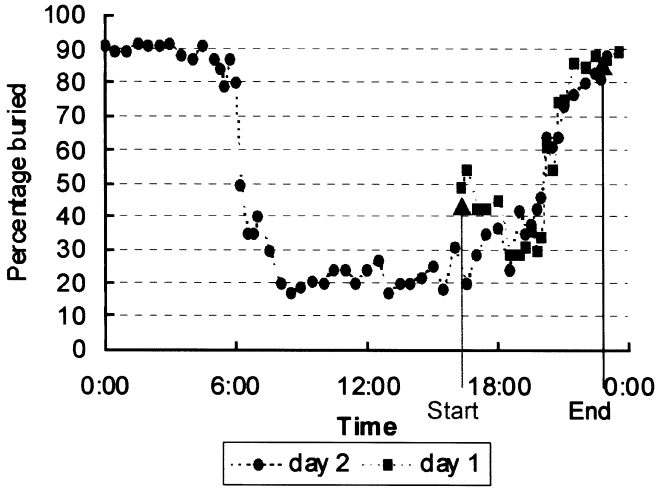

Figure 3: Amount of sandeel burrowed during different times a day.

Figure 3 indicates the day–nigh pattern of sandeel migration. As the figure indicates not all sandeel migrate to the water–column to feed during daytime, but stays in the sediments.

2.1.1 Habitat selection

Sandeels have shown behavior of selecting specific bottom types as their habitat. Research on lesser sandeels in the North Sea indicates that concentration and expansion of sandeel distribution is centered around sites of preferred sediment type [12]. It is argued by Wright et al. that the reason for such a specific choice of habitat, is mainly because of two factors.

First of all the sandeels need a source of oxygen when burrowed in the sediments, even though they can survive with only a small concentration. Since they do not maintain permanent burrow openings, they have to use the interstitial water in the sediment to ventilate their gills. This means that small particles in the in–sediment water could make their gills clog. As a consequence to the fact they need clean oxygen–rich water where they are burrowed, these factors may influence their habitat selection. For the sediment to be oxygen–rich, the sediment needs a hight interstitial water flow. Such sediments are often found at places with constant underwater currents, caused by for example tidal changes. This can also cause depth dependence, when sandeels may avoid deeper water because of less water movement. Optimal depth of sandeels are thought as $30m - 70m$ in the North Sea. Since also particle size is important for both cleanliness and oxygen–concentration, it is though that coarse sediments are preferred over fine particled sediments. When looking at the two sediments silt and sand, the oxygen concentration differs markedly. In silt the oxygen concentration is so low the sandeels would die. On the other hand, sand has almost the same oxygen concentration as present in the water column. Sand should therefore be preferred over silt based on this factor.

Figure 4: Sandeels in their habitat.

The other main factor when sandeels choose their habitat is the ease of sediment penetration. This factor is regarded as key determinant of sediment choice. In studies, the sandeel appeared to favor coarse sand with fine to medium gravel or shell debris $(2 - 16mm)$, more than coarse sand with coarse gravel $(> 16mm)$.

Attempts to predict sandeel distribution from maps of all types of sand, will have over–estimated the extent of sandeel habitat.[12]

2.2 Scattering theory

2.2.1 Introduction

When the sea floor is totally flat and perfectly hard, only one wave will be reflected in a direction symmetrical to the arrival of the incident wave as illustrated in figure 5 (a). This kind of wave is called the specular reflected wave and will reflect no energy back toward the source/receiver, also known as backscattered energy, otherwise for normal reflection. However, a perfectly flat sea floor does not occur in nature, and even small changes in bottom relief can have major influence on the scattering properties of the sea floor. This yields especially for high frequency acoustic waves where the wave length of the acoustic signal often is in the order of the height and curvature length of the sea floor relief.

A more realistic scattering model considers the sea floor as being rough. This rough sea floor will affect the scattering as illustrated in figure 5 (b). From a rough sea floor some energy will be backscattered even for smaller grazing angles. This is because a rougher sea floor makes the scattering more diffuse, meaning a decrease in energy scattered in the specular direction and an increase in scattered energy in all other directions. The more rough the sea floor is, the more diffuse the scattering becomes.

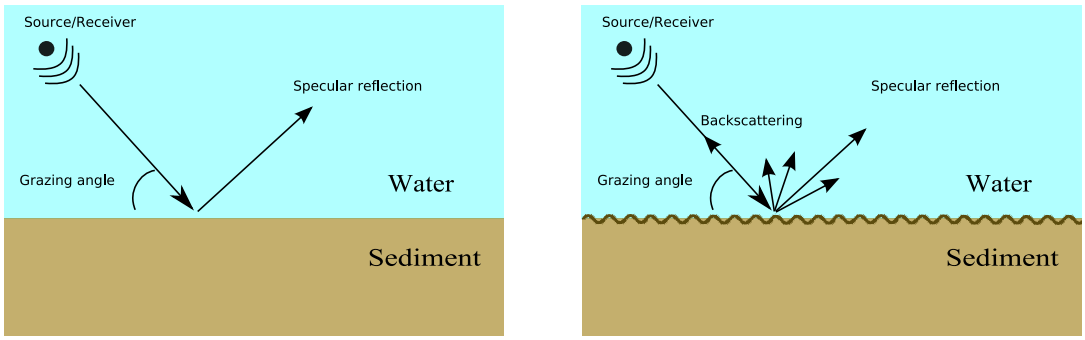

(a) Perfectly hard and flat interface.

(b) Perfectly hard but rough interface.

Figure 5: Scattering from different sea floor properties.

In nature, the sea floor is seldom perfectly hard and even for high frequency acoustic waves some energy will be transmitted into the sediment of the sea floor. This yields especially for softer sediments where the critical angle is small. But since the frequency is high, these waves will be strongly attenuated in the sediment and therefore penetration will be restricted to only a few meters. Nevertheless, additional scattering from the sediment can occur as the wave for example hits objects in the sediment or because of fluctuations in density and refraction indices of the sediment. This situation is illustrated in figure 6.

When considering the situation of figure 6, the total time–dependent intensity measured at the transducer face, $I(t)$, is modeled as the sum of the sediment interface component,

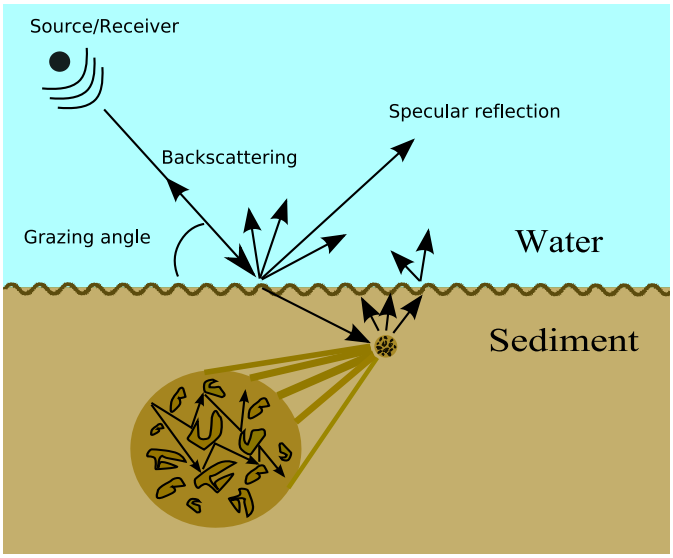

Figure 6: Scattering from a rough sea floor with additional sediment scattering.

$I_{int.f.}(t)$, and the sediment volume component, $I_v(t)$,

$$I(t) = I_{int.f.}(t) + I_v(t). \tag{1}$$

Instead of finding the intensity at the transducer face, the backscattering cross section is more common to find. This parameter is defined as the ratio between the total scattering intensity and incident intensity, multiplied by the square distance r^2.

In *rough* surface scattering, often the scattering cross section *per unit area* is used;

$$\sigma = r^2 \frac{I_s}{I_0 A}. \tag{2}$$

This parameter is dimensionless, but refer to the scattering of a finite patch of the surface large enough to incorporate the essential statistical properties of the surface.

A more convenient quantity is the scattering strength, which is the dB representation of the scattering cross section;

$$TS = 10 \log_{10}(\sigma). \tag{3}$$

Since the backscattering is highly angle dependent, the backscattering cross section of equation (2) will change drastically for different grazing angles. A good model for measuring the backscattering should therefore take into consideration the total aspects of figure 6 for all grazing angles. An example from one such model is given in figure

7. Here the target strength of equation (3) is found for all grazing angles of interest, for both interface scattering and volume scattering. In the figure, roughness scattering first shows a peak near vertical incidence (90° grazing angle). This peak is the remnant of the vertical reflection that would occur if the seafloor were flat. Near the critical angle the roughness scattering shows another peak (around 30°), while decreasing for angles greater than the critical angle. This decrease is a result of a more acoustically "transparent" interface for angles greater than the critical angle. While the roughness scattering decreases for greater grazing angles, the volume scattering increases as a result of the more "transparent" interface. For very soft sediments, where the compressional sound speed tend to be smaller than in water, as example for silt and clay, no critical angle exists. For these sediments the volume scattering tends to dominate roughness scattering at the interface. On the other hand, for very hard sediments the critical angle becomes large, and one should expect less transmitted energy into the sediments and dominating roughness scattering for smaller grazing angles. In fact, it is not clear that a separation into roughness and volume scattering components always is possible or desirable, particularly for seafloors composed of gravel-sized grains or for seafloors whose volume heterogeneity is partly due to vertical undulations of a stratified sediment. Nevertheless, this separation is made in nearly all published models [7].

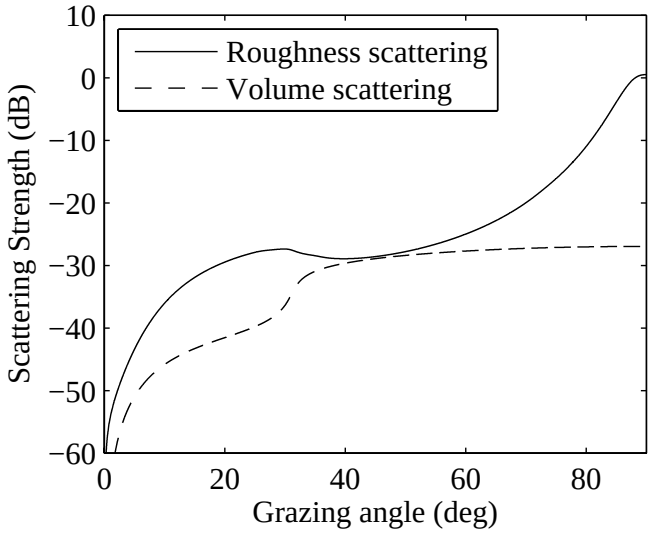

Figure 7: Model example of roughness scattering and volume scattering. The frequency is $30kHz$ and sediment type is coarse sand. The graphs were simulated by using the analytical models of Jackson et al.[6]

To model the scattering from rough surfaces, two different approaches with different theories are mostly used. The first is the Kirchhoff approach (also known as the Helmholtz-Kirchhoff method) and the second is the perturbation approach (also known as the Rayleigh–Rice method). These two approaches have certain constraints as a result of different approximations done – and they do therefore have different regions of validity.

The Kirchhoff approach is considered more accurate for surfaces with large differences in curvature and for angle of incident close to normal. In another word more accurate when the acoustic wavelength is much smaller than the surface height deviations. The perturbation approach is considered a better choice when the height deviations are smaller than the acoustic wavelength and for small grazing angles. An illustrative representation of the regions of validity can be found in figure 8.

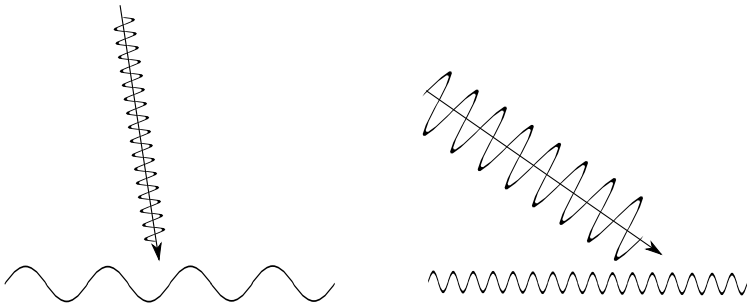

(a) Kirchhoff (b) Perturbation

Figure 8: Regions of validity for the Kirchoff and the perturbation approach.

For the purpose of downward–looking single beam echosounders, the physical properties are most consistent with Kirchhoff scattering theory. The perturbation approach does not consider the coherent (specular reflected) part of the scattering which is important for angles of incident close to normal. When following the theoretical work of Jackson et al.[8], the interface backscatter component corresponding to the *scattered interface component* of equation (1), is obtained from a solution of the Helmholtz diffraction integral using the Kirchhoff approximation. However, a composite roughness approach is used to predict scattering from the sediment volume corresponding to the *volume scattering component*. The reason for using a rough interface scattering approach for finding the sediment volume scattering, is because at high frequencies volume scattering can be treated as an interface process and can be characterized both experimentally and theoretically in the same terms as scattering by seafloor roughness[7]. The basics of the composite roughness approach is the assumption that the sea floor roughness can be treated as a sum of large and small–scale surfaces. Then the backscattering is due to small–scale roughness, with local grazing angle dependent on the slope of the large scale surface.

Theory for both the Kirchhoff approach and sediment volume scattering will be explained in the next sections. For more in depth study on the subjects, recommended reading is the book by Ogilvy [10] or Jackson et al. [7].

2.2.2 Kirchhoff theory

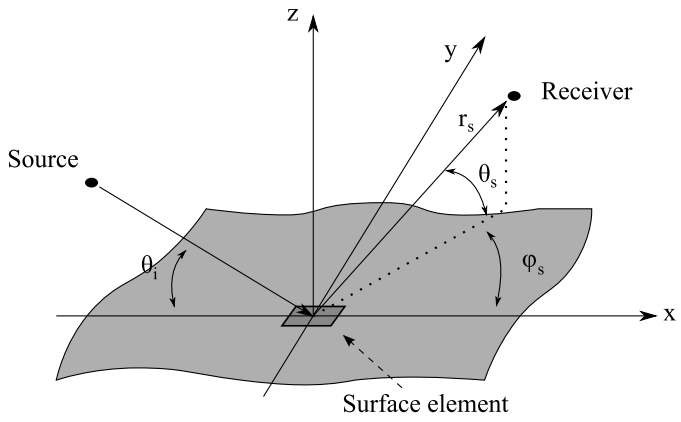

Figure 9: Angular coordinate system used for the Kirchhoff derivations.

The first assumption when finding an expression for the scattering cross section with the Kirchhoff method, is to assume the incident pressure field at the scattering surface as being a plane wave. Then the source needs to be at a great distance from the surface, the far–field, so it produces a plane pressure wave that can be approximated at the interface as

$$P_i = P_{i0} \exp(i\mathbf{k}_i \cdot \mathbf{r}), \tag{4}$$

where P_{i0} is the complex pressure amplitude at the origin, $\mathbf{k}_i$ is the wave number vector giving the direction of propagation and $\mathbf{r}$ is the range vector between the source and the surface element. Considering the angular coordinates of figure 9 and that the plane wave propagate in the x–z plane where $\phi_i = 0$, the incident wave's wave number vector for each coordinate (x, y, z) can be found to be

$$\mathbf{k}_i = \frac{w}{c_w}(\cos\theta_i, 0, -\sin\theta_i). \tag{5}$$

In the equation above, w is the angular frequency of the wave and c_w is the sound speed in water.

For the scattered wave the wave number vector becomes

$$\mathbf{k}_s = \frac{w}{c_w}(\cos\theta_s \cos\phi_s, \cos\theta_s \sin\theta_s, \sin\theta_s). \tag{6}$$

The next assumption, and the most important one, is the Kirchhoff approximation. This approximation, which also is called the tangent plane approximation, considers the rough

surface locally plane. This means that the approximated field at a point on the surface is considered the same as the field present on a tangent plane of that point. When this assumption is made, the reflection coefficient, V_{ww}, can be used at every point on the surface. For this approximation to be valid, the radius of curvature of the roughness must be much larger compared to the acoustic wavelength.

Another assumption that needs to be made assumes the reflection coefficient as being independent of position along the surface. As a result the wave number components are constants. The reflection coefficient can also be replaced by its average value when the surface gradients of the curvature are small, so the variation in angle of incidence only will vary a small amount with surface position.

De Moustier[2] gives a good explaination of the Kirchhoff approximation: "When applying the Kirchhoff approximation the scattered field may be regarded as the summation over the scattering surface of spherically spreading secondary 'sources' from all points on the surface. The amplitude of each source is determined by the local surface gradient and the phase by the local surface height. Diffraction effects are not explicitly included and the phase of each wave is therefore determined by its distance of travel (affected by the surface height) and the amplitude of each wave by the local reflection coefficient."

In a general bistatic situation, the Kirchhoff approximation for the scattering cross section can be written as[7]

$$\sigma = \frac{|V_{ww}(\theta_{is})|^2}{8\pi}[\frac{\Delta k^2}{\Delta K \Delta k_z}]^2 I_K, \tag{7}$$

where the "Kirchhoff integral" is

$$I_K = \frac{\Delta K^2}{2\pi} \int e^{-i\mathbf{\Delta K}\cdot\mathbf{R}}[e^{-\frac{1}{2}\Delta k_z^2 S(\mathbf{R})} - e^{-\Delta k_z^2 h^2}]d^2R. \tag{8}$$

Roughness statistics enter this integral through the "structure function" $S(\mathbf{R})$. This parameter will be explained in more detail later.

The reflection coefficient at the interface, V_{ww}, depends on the choice of wave theory and will in the case of a fluid–fluid boundary be

$$V_{ww} = \frac{z_s - z_w}{z_s + z_w}. \tag{9}$$

Here the reflection coefficient is expressed by using the acoustic impedances z_w and z_s. These impedances represent the relations between the sound pressure and the vertical component of the particle velocity in water and solid media as

$$z_w = \frac{\rho_w c_w}{\sin(\theta_w)}, \tag{10}$$

and

$$z_s = \frac{\rho_s c_s}{\sin(\theta_s)}. \tag{11}$$

The grazing angle θ_{is} for which the reflection coefficient is evaluated at, corresponds to specular reflection from the source to the receiver with the rough surface tilted in such a way as to provide such a reflection. This grazing angle can be written

$$\theta_{is} = \sin^{-1}(\frac{\Delta k}{2k_w}). \tag{12}$$

In equations (7), (8) and (12) both general horizontal components of the wave vectors and wave vector differences are used. These are respectively

$$\mathbf{K}_i = k_w(\mathbf{e}_x \cos\theta_i \cos\phi_i + \mathbf{e}_y \cos\theta_i \sin\phi_i), \tag{13}$$

$$\mathbf{K}_s = k_w(\mathbf{e}_x \cos\theta_s \cos\phi_s + \mathbf{e}_y \cos\theta_s \sin\phi_s), \tag{14}$$

and

$$\Delta\mathbf{k} = \mathbf{k}_s - \mathbf{k}_i, \tag{15}$$

$$\Delta\mathbf{K} = \mathbf{K}_s - \mathbf{K}_i, \tag{16}$$

$$\Delta k_z = k_{sz} - k_{iz}, \tag{17}$$

$$\Delta k^2 = \Delta K^2 + \Delta k_z^2. \tag{18}$$

In order to find the scattering cross section in the backscattering direction, the angles $\phi_s = \pi$ and $\theta_s = \theta_i$ must be replaced in the wave number vectors of equation (5) and (6).

2.2.3 Roughness statistics

When a surface has random roughness, a proper way of describing the surface is by statistical *methods*. Since the acoustical field scattered from the surface also will be a random function, it must be characterized by statistical *parameters*. In practice this has been found to be a difficult task and mean values of the amplitude and intensity of the scattered field are more applicable.

A way of describing the random roughness is by the correlation function of the surface irregularities. This function is generally hard to estimate [4], and it is more convenient to use the wave number spectrum of the relief. The wave number spectrum is the two–dimensional Fourier transform of the correlation function of the surface relief.

In the literature, the two–dimensional roughness statistics are often assumed isotropic with a wave number spectrum following a power–law. This assumption has been made by a number of authors and has showed reasonable good results. Examples are measurements done by Jackson et al. [8] and Essen [3].

The wave number spectrum with the power–law assumption can then be written

$$W(\mathbf{K}) = \beta K^{-\gamma}, \tag{19}$$

where K is the magnitude of the two–way wave vector. This two–way wave vector can be expressed by a single scalar because of the assumption of isotropic roughness, which means that there is no specific directional shape of the bottom (ex. directional sand ripples caused by deep–water currents). The spectral strength β and the spectral exponent γ are both structure parameters of the bottom and depend upon the roughness characteristics. β influences the amplitude of the roughness relief, while γ influences the composition of different structure components, resulting in the total roughness relief of the surface.

As seen from equation (19), the power spectrum decreases with the roughness wave number. This is because when the wavelength of the relief is long, the amplitude is thought as larger, than when the wavelength is short. This is illustrated in figure 10.

The power–law function of the roughness spectrum is related to the structure function $S(\mathbf{R})$. This function gives the variance of the height deviations for fixed horizontal displacement, and can be easier to interpret than the power spectrum. The power–law spectrum and structure function is connected by the following transform

$$S(\mathbf{R}) = 2 \int (1 - \cos \mathbf{K} \cdot \mathbf{R}) W(\mathbf{K}) d^2 K. \tag{20}$$

When isotropic roughness is assumed, the structure function depends only on the horizontal distance R between elements on the surface and the wave number K (magnitudes

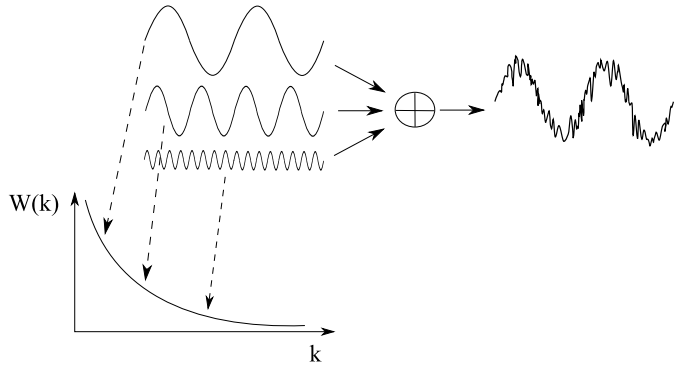

Figure 10: Decomposition of the amplitude of a random rough surface into spectral components.[9]

of the two–dimensional vectors **R** and **K**), and can then be written when applying the power–law spectrum of equation (19) as

$$S(R) = C_h^2 R^{2\alpha} \tag{21}$$

where

$$C_h^2 = \frac{[2\pi\beta\Gamma(2-\alpha)2^{-2\alpha}]}{[\alpha(1-\alpha)\Gamma(1+\alpha)]} \tag{22}$$

and

$$\alpha = \frac{\gamma}{2} - 1. \tag{23}$$

Γ is the Gamma function and the parameter α is restricted to the interval $0 < \alpha < 1$.

With this restriction to α, γ of equation (19) must lie within the interval $2 < \gamma < 4$. For high frequency bottom scattering, appropriate values lie within the region $3 < \gamma < 3.5$. [8]

To give an example of how the structure function describes the sea floor, assume $\gamma \approx 3.25$ and $C_h R^\alpha \approx 3cm$. These values of γ and the square root of the structure function (proportional to the standard deviation of the roughness) are found reasonable for $r = 100cm$. This means that for points separated a distance of $100cm$ from each other on the sea floor, the rms height deviations are approximately $3cm$. When it is assumed that the power–law holds at larger scales, the rms height deviations increases rather slowly as function of the distance between separated points, being approximately $60cm$ at $100m$ and $2.5m$ at $1000m$. Topographic changes of this magnitude are quite reasonable. [8]

2.2.4 Power–law Kirchhoff approximation

When isotropy is assumed, the structure function introduced will only depend on the magnitude, R, and the two–dimensional wave number will only depend on the magnitude, K. Then the Kirchhoff integral can be reduced to a one–dimensional integral by transforming to polar coordinates and performing the angular integral. In addition if the power–law structure function is used, the kirchhoff integral becomes

$$I_K = \int_0^\infty J_0(u) e^{-qu^{2\alpha}} u du \tag{24}$$

where

$$q = \frac{1}{2} C_h^2 \Delta k_z^2 \Delta K^{-2\alpha}. \tag{25}$$

A numerical approximation for the scattering cross section of equation (7) in the backscattering direction when applying the assumptions of equation (24), can be found in appendix A. In addition, figure 11 gives an example of this numerical solution for the Kirchhoff approach for steep grazing angles at different frequencies.

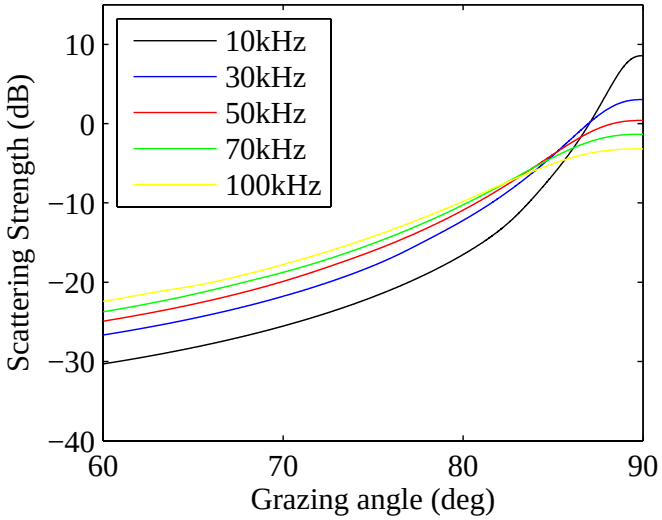

Figure 11: Numerical results for roughness scattering estimated by Kirchhoff approximation. Bottom type is coarse sand. Only the frequency of the acoustic signal is changed between different plots.

As can be seen from the figure, there will be a frequency dependency of the scattering strength which changes for different grazing angles. In the figure the power–law function is applied with a scattering exponent of $\gamma = 3.25$. When this spectral exponent is applied

and the frequency increases, the backscattering will decrease – especially for greater grazing angles. This is also the physically behavior one would expect of the scattering in nature, when a higher frequency "sees" the surface as more rough compared to smaller frequencies – making the scattering more diffuse for higher frequencies.

When changing a parameter of the sea floor properties instead, like the rms heights of the roughness relief, as for different frequencies the scattering strength in the backscattered direction changes. This can be seen in figure 12 where all other parameters than the rms relief heights are held constant.

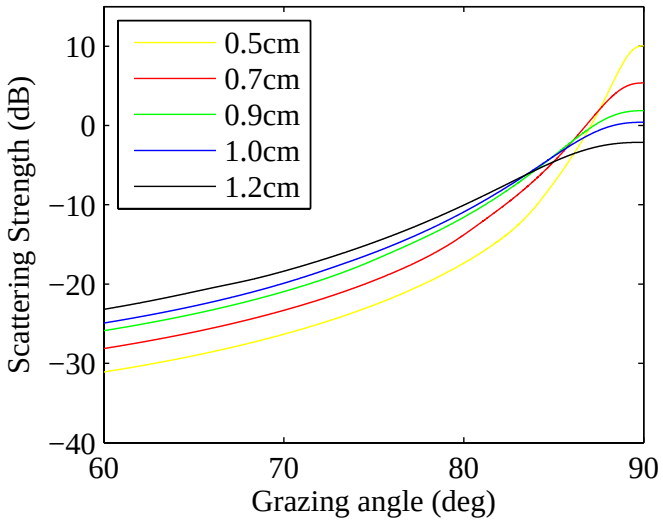

Figure 12: Numerical results for roughness scattering estimated by Kirchhoff approximation. Bottom type is coarse sand. Only the rms roughness height is changed between different plots. A frequency of $50kHz$ was chosen.

In many ways the scattering strength for different rms heights changes as for different frequencies. When the rms height increases, the scattering strength decreases – especially for larger grazing angles. This can be understood by more diffuse scattering for higher roughness reliefs. As explained for an increasing frequency, the acoustic signal "sees" the surface as more rough for higher roughness reliefs. Then the angle dependency of the scattering becomes more even.

2.2.5 Sediment volume scattering

When finding an expression for additional sediment volume scattering for a fluid sediment model, first some assumptions need to be made for the sea bottom properties. First of all the average complex compressional sound speed and density of the sediment must be constant with respect to depth. This assumption is usually fulfilled when the acoustical frequency is high and grazing angles low - in another word where acoustic penetration depths are small enough not to expose sediment layering. However in some cases problems can occur for higher frequencies above approximately $100kHz$, where the first millimeters below the interface can cause gradients in physical properties. Second, attenuation in the sediment limits penetration to depths that are much smaller than the distances from the source and receiver to the scattering region. This assumption enables the penetrating wave to be assumed plane over the total volume scattering region. The third assumption is that the incident field on the interface is much larger than the scattered field in the sediment volume, making sediment volume scattering an interface process. The last assumption is to neglect scattering effects of the sediment–water interface, in another word neglect scattered energy at the interface from the sediment volume back to the water column.

If all the assumptions are fulfilled, the backscattering cross section for the sediment volume can be found by the formula[5]

$$\sigma_{svs}(\theta) = \frac{\sigma_v \left|1 - V_{ww}(\theta)^2\right|^2 \sin^2\theta}{4k_w \left|P(\theta)\right|^2 \Im\left[P(\theta)\right]}, \tag{26}$$

where

$$P(\theta) = \sqrt{\kappa^{-2} - \cos^2\theta} \tag{27}$$

and

$$\kappa = \frac{1 + i\delta}{\eta}. \tag{28}$$

In equations (26) to (28) k_w is the horizontal wave number in water, $V_{ww}(\theta)$ is the reflection coefficient between the boundary of two fluid media, σ_v is the volume scattering cross section, δ is the loss tangent (attenuation) of the sediment and η is the ratio between the compressional sediment sound speed and water sound speed. The imaginary part of equation (26) determines the wave's dissipation in the sediment.

One thing to note about equation (26) is the fact that there will exist some sediment scattering for subcritical grazing angles, which also is the case in nature.

The volume scattering cross section σ_v is most simply found empirically by data fitting rather than by theoretical calculation. One such approach uses a dimensionless parameter to find the sediment volume scattering[6]

$$\sigma_s = \frac{\sigma_v}{\alpha_s}, \tag{29}$$

with the value of σ_s lying between 0.0001 and 0.004 and α_s as the absorption coefficient of the sediment. If σ_s is taken to be frequency independent, then equation (26) will yield a scattering cross section that is nearly frequency independent[7].

Equation (26) for the volume scattering cross section is only applicable for flat surfaces. Since a rough interface will alter the field entering the sediment from that expected for a flat interface, some modulations of the equation are needed. One option is to use an approximation analogous to the composite roughness model[7]. For this model account is taken of the larger-scale slope of the sea floor by averaging the volume scattering cross section over the expected distribution of local grazing angles. The local grazing angle is dependent on the local value of the large–scale slope. This principle is illustrated in figure 13.

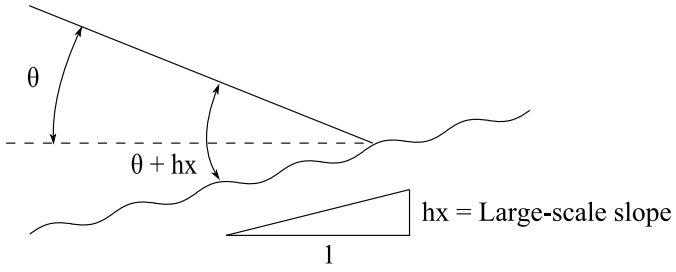

Figure 13: Large–scale slope averaging process used in the composite roughness model.

If the rms value of the large scale surface is small

$$s < 0.1, \tag{30}$$

and the grazing angle is not too large ($\theta < 70$), then the local grazing angle pictured in figure 13 can be approximated as $\theta + hx$.

When the large–scale slope is assumed being a Gaussian–distributed random variable with standard deviation s, the volume scattering cross section is obtained as an average over the large-scale slope as follows[8]:

$$\sigma(\theta) = \frac{R(\theta, s)}{\pi^{\frac{1}{2}} s} \int_{-\theta}^{\infty} \sigma_{svs}(\theta + hx) \exp\left(-\frac{hx^2}{s^2}\right) dhx \tag{31}$$

The function $R(\theta, s)$ accounts for shadowing by the large–scale surface. A shadowing function that can be used is

$$R(\theta, s) = (2Q)^{-1}(1 - e^{-2Q}), \tag{32}$$

where

$$t = s^{-1} \tan(\theta), \tag{33}$$

$$Q = (\frac{1}{4t})[\pi^{\frac{1}{2}} \exp(-t^2) - t(1 - erf(t))], \tag{34}$$

and erf is the error function.

2.3 Depth compensation

In the water column, the transmitted pulse will be affected by spherical spreading loss and absorption. The shape of the received pulse will therefore be highly dependent upon the pulse's distance of travel, or in another word the water depth. Also the received pulse will be elongated or compressed as function of time, when the water depth is changing. These effects are shown in figure 14.

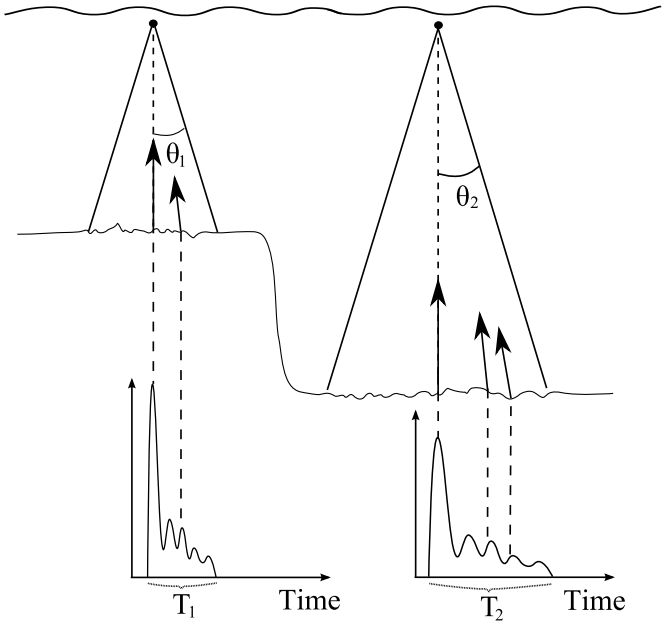

Figure 14: Depth dependence of received signal.

The figure describes how the received pulse changes for two different water depths for the same beam width $2\theta_1 = 2\theta_2$. As can be observed, the amplitude of the received signal decays for a greater water depth as a result of loss and absorption. Another observation is that the duration of the received pulse T gets smaller for shallower water ($T_1 < T_2$). This is because of different path lengths of the backscattered pulse for different depths.

When comparing or averaging a selection of pings over various depths, the mentioned effects must be compensated for. This is best done by time and power corrections. Time correction is made to adjust the duration of the received pulse while power correction removes the effects of spherical spreading and absorption.

2.3.1 Time correction

When sampling the received signal of each ping, the sampling is done at equal time intervals. This is a problem when the depth changes – because more samples are obtained for a certain angle for deeper depths in comparison to smaller depths. The shape of the received signal can then change even if the type of object causing the echo stays the same. Time correction is done by resampling the received signal to a reference depth, and will remove the need to allow for beam patterns and for the backscatter function changing with angle of incidence.

The time adjustement factor is

$$\gamma = \frac{d}{d_0}, \tag{35}$$

where d is the actual sea floor depth and d_0 is the reference depth.

Then the corrected time will be

$$t_{corr} = \frac{t}{\gamma} = \frac{d_0 t}{d}, \tag{36}$$

where t_{corr} is the corrected time and t is the uncorrected time.

After depth is adjusted for, interpolation is performed at times corresponding to reference depth sample times.

2.3.2 Power correction

When compensating for spherical spreading and absorption, a Time–Varying Gain (TVG) function can be used. This function is adapted to the physical law of target echo level variation. For volume targets this function can be written

$$TVG = 20\log_{10}(R) + 2\alpha(R), \tag{37}$$

where α is the absorption coefficient in dB/m for the specific acoustic frequency and R is the range in meters.

There should be emphasized that the TVG function does not increase SNR – both noise and signal level will simultaniosly be affected.

2.4 Volume scattering strength – Sv

The volume scattering strength, Sv, is converted from received power values by the following equation:

$$\begin{aligned} Sv &= P_{recv} + 20\log_{10}(r) + (2\alpha r) \\ &\quad -10\log_{10}\left[\frac{P_{xmit}\cdot(10^{G/10})^2\cdot\lambda^2\cdot c_w\cdot\tau\cdot 10^{\psi/10}}{32\cdot\pi^2}\right] \\ &\quad -2\cdot Sa_{corr}, \end{aligned} \tag{38}$$

where P_{recv} is received power, r – range, α – attenuation in water, P_{xmit} – transmitted power, G – gain, λ – acoustic wave length, τ – pulse length, ψ – equivalent beam angle and Sa_{corr} – correction for Sa.

The expression on first line of equation (38) constitute compensation for spherical spreading and absorption. This expression is known as the TVG function. Next, the second line constitute compensation for all gains while the expression on line three compensates for spherical abberation.

2.5 Averaging

Averaging of pings together constituting a pingset can be performed by the following equation

$$p_{avg}[n] = \frac{1}{M} \sum_{m=0}^{M-1} p[m, n], \tag{39}$$

where p is amplitude values, $n = 0, 1...N-1$ represents samples per ping and $0 < m < M-1$ represents pings. Sample based averaging should only be performed after depth normalization of the pings to be averaged.

2.6 Smoothing

To reduce noise, additional smoothing of a signal can be performed by three–point weighted averages. This equation becomes

$$p(n') = \sum_{n=0}^{N-1} 0.25 \cdot p(n-1) + 0.5 \cdot p(n) + 0.25 \cdot p(n+1), \tag{40}$$

where p is amplitude values, $n = 0, 1...N-1$ represents samples of a ping and $n' = 0, 1...N-1$ represents smoothed samples.

3 Data acquisition and survey execution

3.1 SMASSC

The **S**urvey **M**ethods for **A**bundance Estimation of **S**andeel (Ammodytes marinus) **S**to**c**ks (SMASSC) project was initiated by the Reaserch Council of Norway and is a co–operation between the Institute of Marine Research (IMR), DIFRES (Denmark) and the University of Bergen. The main reason for excexution of the project is hence to the critically state of the sandeel stock in the North Sea and the International Council for the Exploration of the Sea (ICES) has addressed urgent need for scientific survey time series in this area, as a result of insufficient assessment. The aim for the SMASSC surveys is to improve the assessment and increase the general knowledge of sandeel using new technology, when the current status of sandeel assessment is based solely on rather unreliable commercial fishery data. For the application advanced acoustic technology and the use of several catching devices for sandeel buried in the sediments are planned being used. This is needed to develop a robust survey design for abundance estimation, when conventional standard survey techniques are insufficient to assess the sandeel stock due to the complex behaviour of the species.

Three trial surveys are planned during a three weak period in 2008–2010 from late April to mid May, the main fishing season on sandeel in the North Sea. One of the IMR owned vessels R/V Johan Hjort or R/V G.O.Sars will be used for the surveys and will be holding the standard survey equipment, including a small commercial sandeel trawl gear.

3.1.1 Survey execution 2008

For the 2008 SMASSC survey, the vessel S/V Johan Hjort was used. This vessel is equipped for fisheries and environmental research. The equipment onboard includes advanced acoustic instruments for fish detection and echo integration, gear for operating various types of mid–water and bottom trawls, various types of plankton samplers and other equipment for environmental observations.

Acoustic data and sandeel samples were collected mainly in two different areas. These two areas were “Vestbanken” and “Elbow Spit North” and their location can be found in figure 16. Both areas are typical sandeel fishing grounds.

Figure 15: S/V Johan Hjort

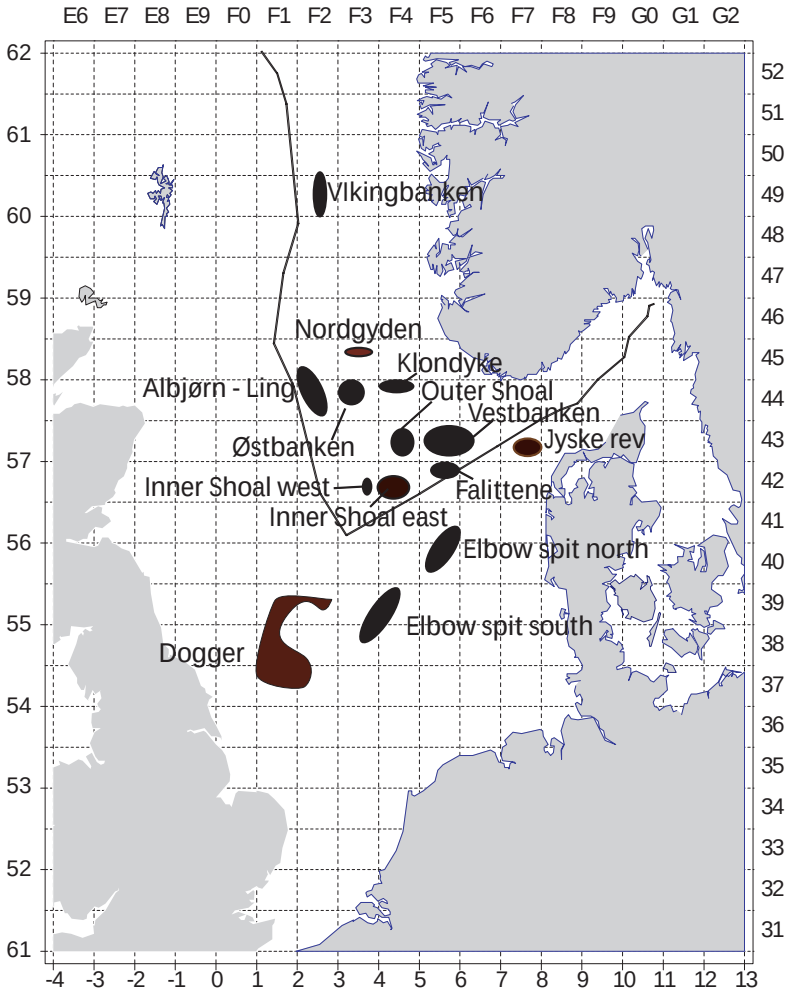

Figure 16: Sandeel fishing grounds in the North Sea.

Acoustic Equipment

- Specifications:

  A calibrated Simrad ER500 multi–frequency echosounder was constantly collecting data on the frequencies $18kHz$, $38kHz$, $120kHz$ and $200kHz$. To view the echograms of the different channels, the Simrad ER60 software was connected to the echosounder. More detailed specifications on operating parameters of Simrad's ER500 will be given later.

  In addition to the ER500 echosounder, the Simrad SH80 omnidirectional high frequency sonar was used. This is a multi–beam echosounder and has the potential of observing the whole water volume around the vessel.

- Purpose:

  Acoustic surveys offer continious, high–resolution observations through the water column, providing a spatial and temporal data richness that cannot be achieved by conventional point sampling methods such as trawls, grabs and dredges.

  After proper detection, accurate species identification is needed. Multi–frequency information claims to give much more accurate identification, in particular for organisms with no gas inclusions or swimbladder. Initial trials of dual frequencies and at multiple frequencies 18, 38, 120 and 200 kHz on sandeel have shown that identification is possible, and that a relative frequency response, can be used as a good candidate for statistical species seperation.

  For converting acoustic data to biomass, proper data on the target strength of the organism is also needed. Individual target strenght measurements at one frequency can be found by trapping sandeels in modified cages on the bottom equipped with video and a 120 or 200 kHz split beam transducer.

Sampling Equipment

- Grab:

  The van Veen grab has been designed for quantitative sampling of benthnic invertebrates. This sampling device has also been shown to be efficient in estimating density of sandeel buried in the seabed. A video camera can be mounted on the grab, in order to quantify the problem of avoiding sandeel during the closing face of the grab. Otherwise, it is assumed that the grab has close to absolute sampling efficiency. Picture of a grab can be found in figure 17.

Figure 17: Grab

- Sledge:

  The sledge is equipped with teeth that penetrate into the sediment to trigger the fish to emerge from being buried in the seabed. A video sledge can be used to study the escape behaviour of sandeel. Picture of a sledge can be found in figure 18.

Figure 18: Sledge

- Trawl:

  For scientific sampling, a full commercial sandeel trawl can be used. In order to reduce catch rates and enable multiple school samples in one tow, the trawl can be equipped with a multiple cod end system.

Figure 19: Trawl

3.2 Transducer specifications and possible limitations

An overview of the different parameters for the transducers of the ER500 echosounder used to collect the echo data for this project, are given in table 1. More detailed information about the different transducers can be found in the data sheets in appendix B. In addition, general operating parameters for all transducers can be found in table 2.

Table 1: Transducer specifications

Parameter	**18kHz**	**38kHz**	**120kHz**	**200kHz**
Type	ES18–11	ES38B	ES120–7	ES200–7
Gain	$22.72dB$	$26.67dB$	$23.73dB$	$26.97dB$
Sa Corr	$-0.58dB$	$-0.58dB$	$-0.35dB$	$-0.30dB$
2–way beam angle	$-17.10dB$	$-20.60dB$	$-20.80dB$	$-20.70dB$
Angle sensitivity, along	13.90	21.90	21.00	23.00
Angle sensitivity, athwart	13.90	21.90	21.00	23.00
Angle offset, along	$-0.04°$	$-0.05°$	$0.03°$	$0.05°$
Angle offset, athwart	$0.03°$	$0.12°$	$0.06°$	$-0.02°$
Beam width, along	$10.96°$	$7.17°$	$7.38°$	$6.63°$
Beam width, athwart	$11.01°$	$7.18°$	$7.16°$	$6.53°$
Receiver bandwidth	$1.57kHz$	$2.43kHz$	$3.03kHz$	$3.09kHz$

Table 2: General parameters

Parameter	Value
Pulse duration	$1024\mu s$
Sample interval	$0.189m$
Transducers depth	$8.00m$
Transducers beam type	Split

The sample interval is here given in meters. For converting this parameters into time, $t = 2 \cdot r/c_w$ might be used, where r is range and c_w is the sound speed in water. The directivity beam patterns for each of the transducers used, can be found in figure 20. Every circular sector represents an angular difference of 10°. When receiving the bottom echo for the different frequencies, and performing analysis of the received echoes, the beam pattern may influence the received echo–shape and must be considered.

In an ideal situation, when characterizing the sea floor based on the received echo, the beam width should be large enough to pick up all scattering from oblique angels. Hamilton proposes a beam width of 12° and less may be too narrow for good acoustic bottom classification, and may not be sufficient to receive the tail [1]. As can both be seen from the transducer beam patterns in figure 20 and from the transducer specifications

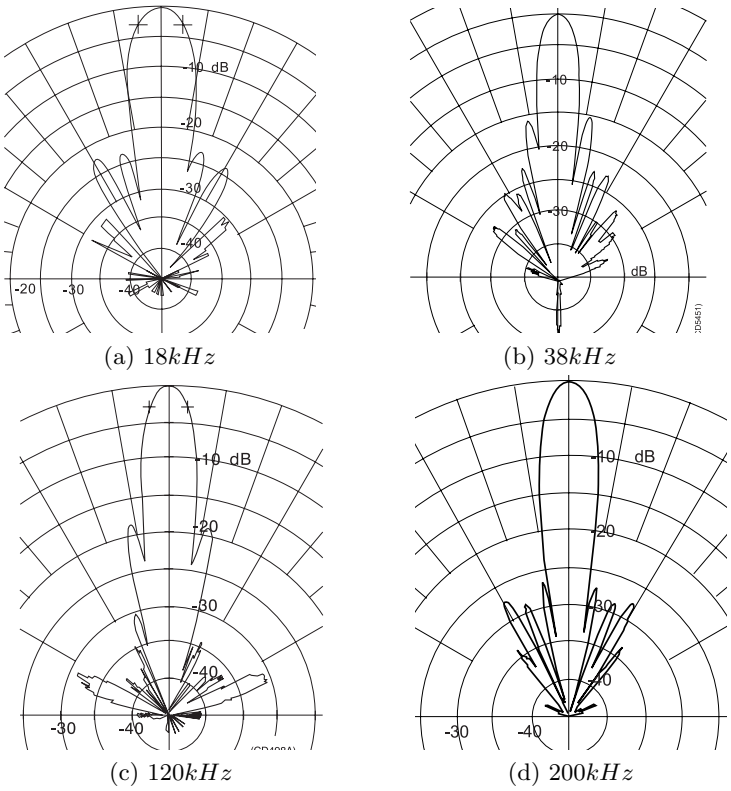

(a) $18kHz$ (b) $38kHz$

(c) $120kHz$ (d) $200kHz$

Figure 20: Directivity beam patterns for the different transducers. Every circular sector difference is 10°.

in table 1, none of the transducers have a wider beam width than 12°. The reason for a narrower beam width is because of the application the transducers are designed for, which is fish detection. However, it would definitively be an advantage if the same transducers could be used for both fish finding and bottom classification. This is the scope of this project – and anyhow it is not to design a full bottom classification system, but try to determine typical sandeel grounds.

As mentioned introductorily and as a result of quite narrow beam widths, the side lobes may be brought into play when analysing the tail of the received bottom echoes. In figure 21 on the next page, an example of an averaged received bottom echo for each of the different frequency channels can be found.

As can be observed in the figure, especially for the $200kHz$–channel, a drop in Sv level occur at the end of the main peak. This drop occur at approximately 48 meters for this channel. Even though not a totally correct elucidation, when assuming the first echo arrive at normal incidence and a depth of approximately 45 meters, the angle of departure can be found to be 3.8°. When looking at the beam pattern of the $200kHz$ transducer in 20 (d) and considering the beam width of 7° ($2 \cdot 3.5°$), the dip is most probably

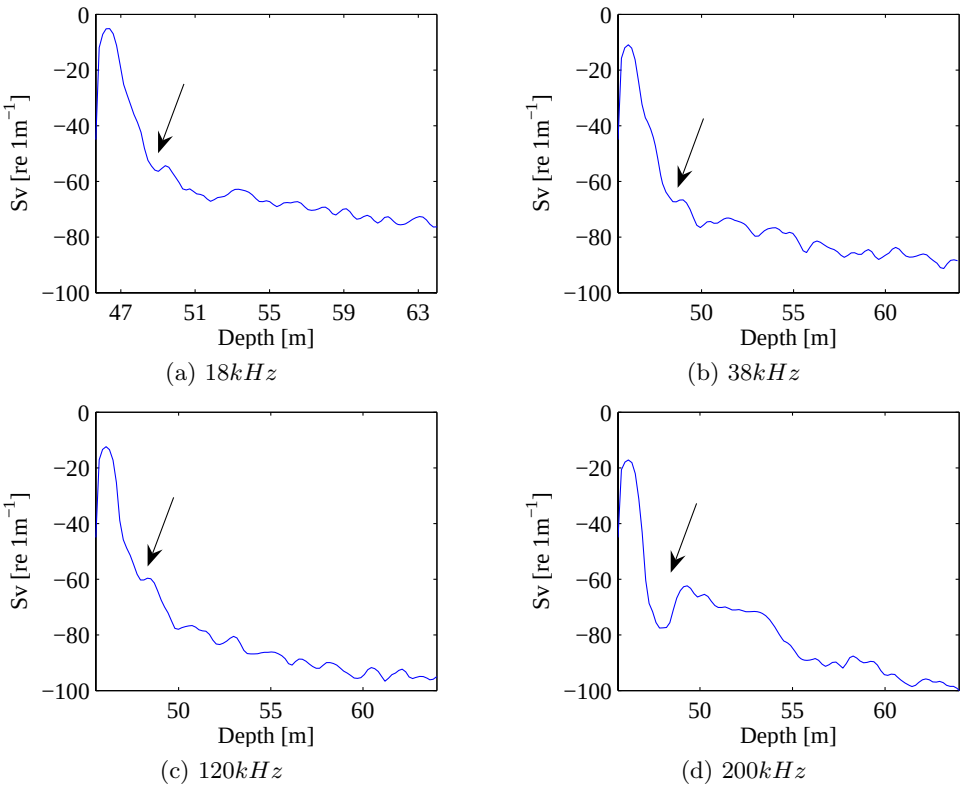

(a) $18kHz$ (b) $38kHz$

(c) $120kHz$ (d) $200kHz$

Figure 21: Received bottom echo for different frequencies. Arrows indicate possible beam pattern minima.

caused by the minima between the main lobe and the first side lobe. At approximately 55 meters the tail fades out and when performing the same calculation as above, the angle of departure is found to be 12.5°. This corresponds to the end of the first side lobe in 20 (d). As a summary, the scattering at oblique angles for the $200kHz$–channel is actually received by the first side lobe and not by the main lobe. This is somewhat an idealized assumption, when multiple scattering effects and sediment scattering also can contribute to the tail. Since the first side lobe is much lower than the main lobe, noise could be a problem. However, by the ER60 software the noise level was measured to no more than $-110dB$ to $-120dB$ and considering the tail lying in the region $-60dB$ to $-80dB$, these values are well above the noise level.

The same situation as for the $200kHz$–channel occur for the other channels as well, though not as clear. A small dip followed by a small peak can be observed where the main lobe has fallen a certain amount of dB in 21 (a), 21 (b) and 21 (c). When performing the same calculations as in the previous paragraph, these dips are results of the first side lobes found in their beam patterns.

Be aware that the depth in figure 21 is measured from the transducers and not from

the sea surface. Since the echosounder is mounted on the ship's hull, there will be a difference of some meters between the sea surface and the echosounder. The transducer depth in this project can be found in 2 on page 30. In the rest of the report, for all *processed* echoes, the depth will always be measured from the transducers.

3.3 SEABEC results

Kongsberg's EA 400/600 Seabed Classification Software (SEABEC) was used in order to distinguish between what could be areas of typical sandeel grounds from areas of other sea bed properties, in both "Vestbanken" and "Elbow Spit North". The classification software computes the roughness and hardness of the sea floor, based on the differences between the first echo received from the sea floor at the frequencies $38kHz$ and $200kHz$. An indepth procedure for analyzing the received echoes stays a product secret, however as in other commercial sea bed characterization systems multivariat analysis is the main characterization method. The result from SEABEC is plotted as color–points on the ship's path, where different color gradations represent the degree of either roughness, hardness or both roughness and hardness together.

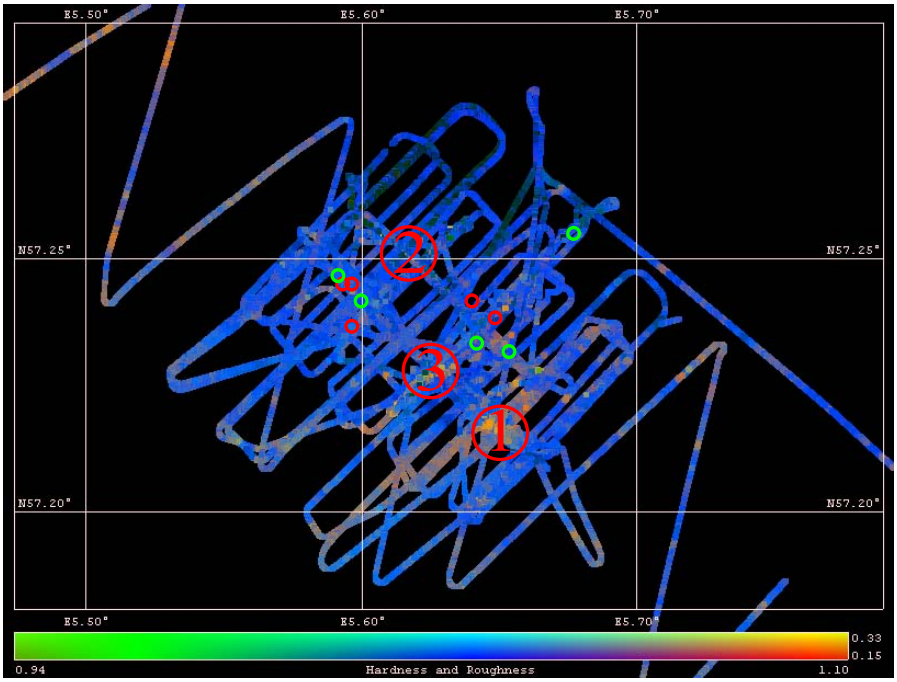

Figure 22: Hardness and roughness of "Vestbanken".

The result from "Vestbanken" of both roughness and hardness together, is given in figure 22. Be aware that the color gradations are scaled to the specific area and are therefore not global. Irrespective of the scaling, there is possible to distinguish between areas of different hardness and roughness. Yellow color indicates the areas of the greatest hardness and roughness, blue indicates the areas of moderate, while dark green indicates the areas of least hardness and roughness. In addition, three regions are highlighted with numbers one to three. In these three regions, the major findings by sledge samples were found during nighttime. Region number one had the largest catch–size of 441 sandeels, while region number two had the 2nd largest of 177 sandeels. From the total of nine

different sledge samples containing more than ten sandeels, region number one had the largest, 3rd, 4th, 8th and 9th largest finding, region number two had the 2nd and 5th, while the third region had the 6th and 7th largest finding. The total overview of findings in the different regions can be found in table 3. Region number one was the only region without any findings less than ten sandeels from the sledge samples. In the figure, also findings outside the three regions of less than ten sandeels and of zero sandeels are plotted respectively as red and green circles. The difference between the three regions individually and difference from samples outside the regions, can indicate preferred sandeel grounds. Especially region one stands out as an area of large findings and a consistent rough and hard sea floor. This can indicate the possibility of this region as a preferred sandeel ground. On the other hand, region two looks like having less roughness and hardness, but had the 2nd largest finding.

Table 3: Sledge catch–size during night for the different areas of "Vestbanken".

Number	Catch–size	Region
1	441	1
2	177	2
3	133	1
4	54	1
5	40	2
6	37	3
7	21	3
8	15	1
9	14	1

In addition to the figure of hardness and roughness together, seperate figures of hardness and roughness from "Vestbanken" can be found in figure 23 and 24. The color–scale goes from light green, via blue, to dark red. Light green indicates areas of lesser roughness or hardness while red indicates areas of more roughness or hardness. Both figures support the concentrated hardness and roughness estimates of region one. The large findings in region two stays inexplicable, when this region has lesser roughness and hardness than both region one and three.

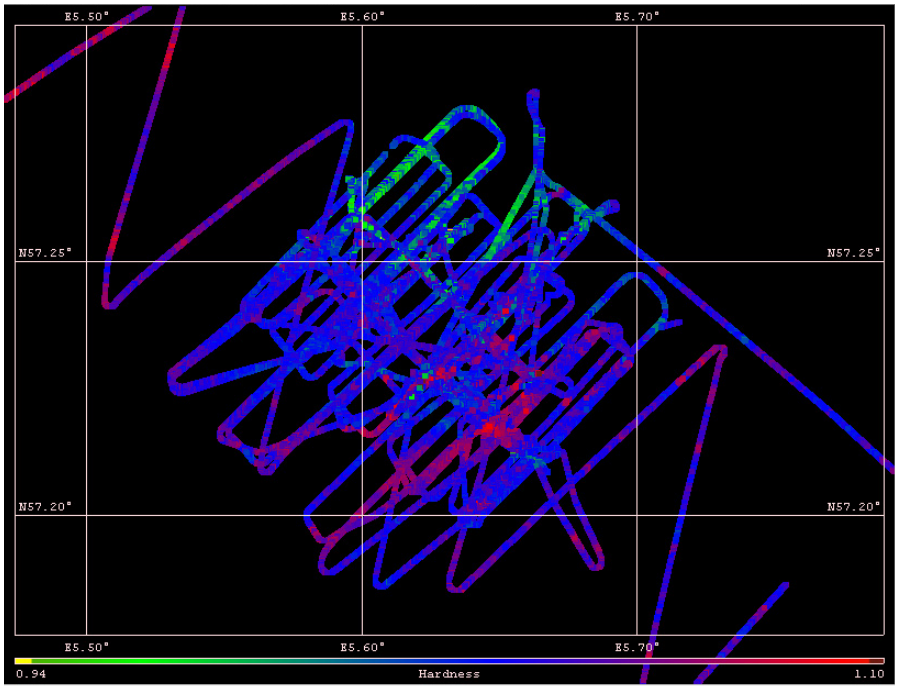

Figure 23: Hardness of “Vestbanken”.

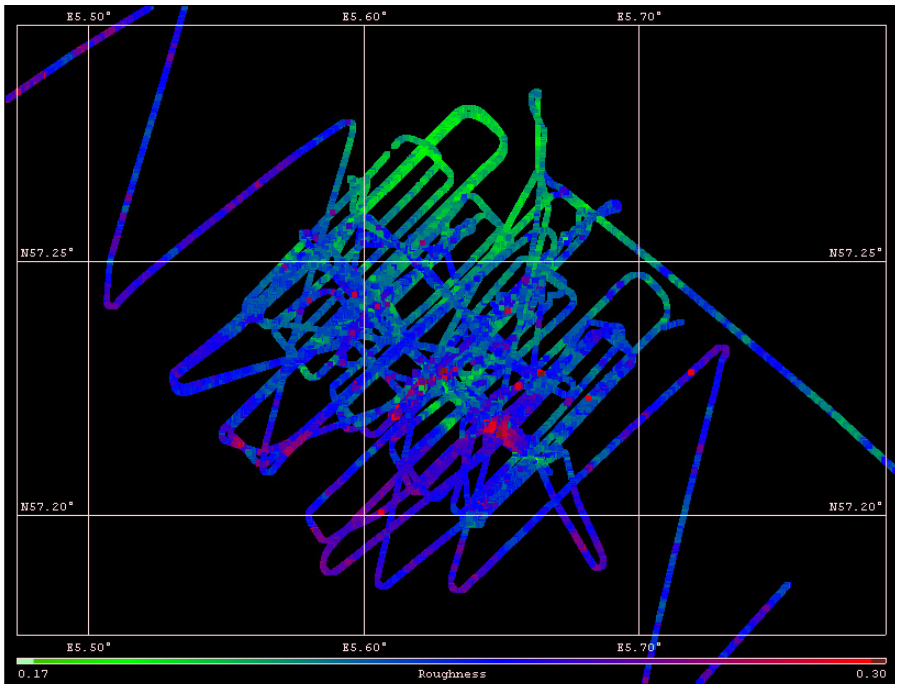

Figure 24: Roughness of “Vestbanken”.

For survey area two which was “Elbow Spit North”, hardness and roughness together can be seen in figure 25. The findings of the different regions indicated in the figure can be found in table 4.

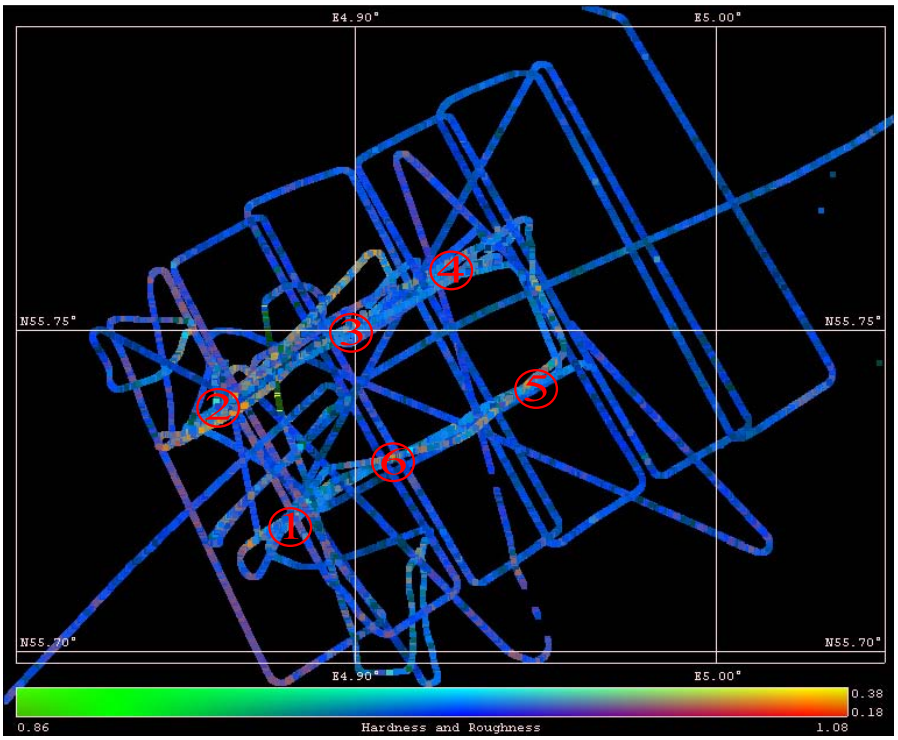

Figure 25: Hardness and roughness of “Elbow Spit North”

There is harder to observe differences in hardness and roughness for “Elbow Spit North”. In addition SEABEC seems to characterize the sea floor roughness and hardness different for overlapping ship paths at some locations. This is easiest seen in the roughness plot of figure 27. The settings of the program were the same for both “Vestbanken” and “Elbow Spit North”, and therefore the reason for overlapping ship path differences of “Elbow Spit North”are hard to explain. The differences might have come from the fact that only pings from “Vestbanken”were used for calibration of the SEABEC system, but this is hardly the main or only explanation. Because of the differences and possible ambiguities, no further discussions of the different regions and their findings will be made for this area.

The findings of SEABEC support the multi–frequency potential of characterization of sandeel grounds, as region one from “Vestbanken” indicates. However there exist no conclusions from the SEABEC results, because of the differences in hardness and roughness of the different areas where sandeels were found. There is anyhow a possibility that a system designed for locating sandeel grounds would give a better result, when such a system could be calibrated for such purpose.

Table 4: Sledge catch–size during night for the different areas of “Elbow Spit North”.

Number	Catch–size	Region
1	178	1
2	168	3
3	85	2
3	85	4
4	83	6
5	58	4
6	53	2
7	51	3
8	32	6
9	12	5

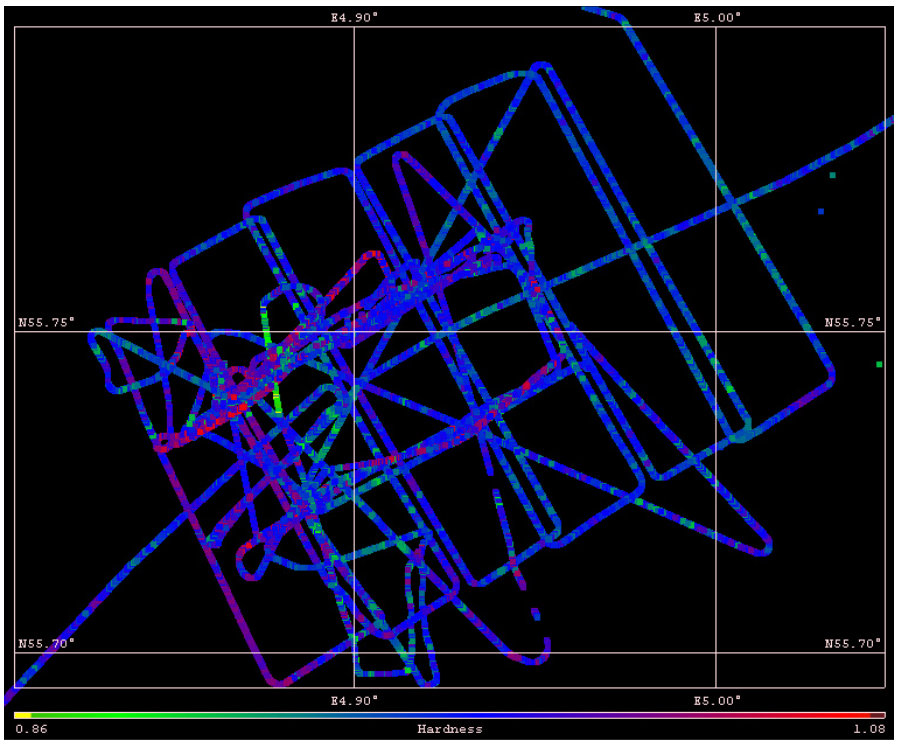

Figure 26: Hardness of “Elbow Spit North”.

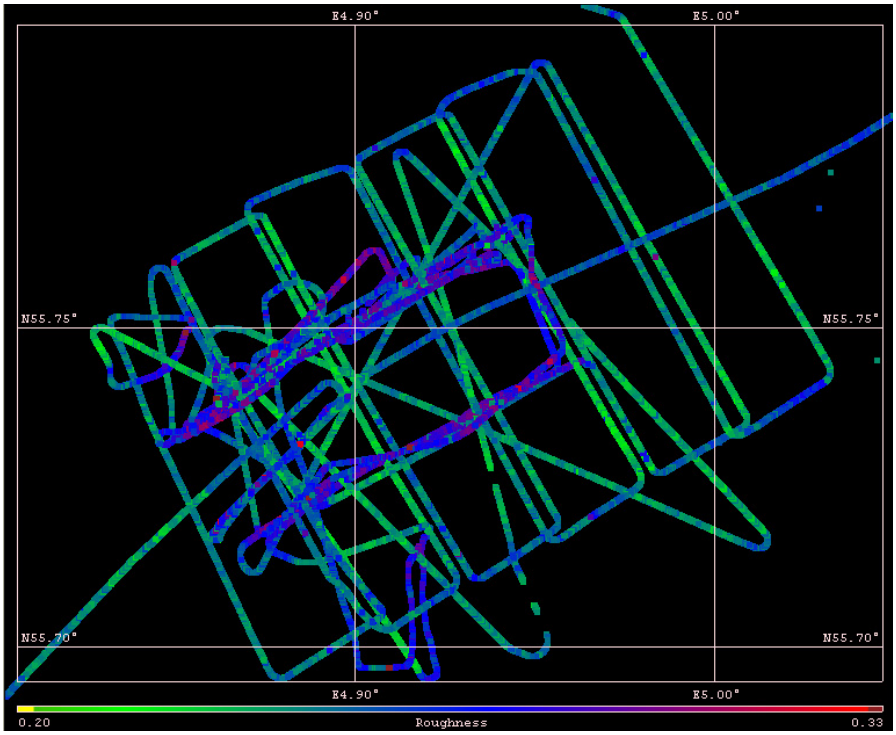

Figure 27: Roughness of “Elbow Spit North”.

4 Signal processing

All signal processing in this report were done in Matlab. Toolkit of reading routines for echosounder *.raw* data were provided by Institute of Marine Research in Bergen. This toolkit reads data from all frequency–channels and different output is given for different input specifications.

The next section will explain step by step all the processing that were made to provide the results of different echo parameters presented later. There will not be given any explanation of the toolkit provided by IMR. Refer to the attached CD for Matlab scripts of all processing routines developed during this project and detailed explanations of the scripts.

In this report Sv values were used for phenomenological analysis of sea floor echo–shape. However, there should not be causing any major problems by using for example power values instead when characterizing the sea floor echo, as long as the data is calibrated and compensation for depth is utilized. The echo shape stays the same irrespective of what value chosen, but there will be a difference in levels. Most important dB values must be used, because of large differences between received linear values in every ping. However, this report will not try to evaluate other values than Sv values and when comparing or using the results of this report, Sv values should be used.

4.1 Bottom pick and echo alignment

The first approach for the classification is to locate the first bottom echo from the total signal received for each ping. This is actually one of the most crucial parts of the signal processing and has to be done with care. It is important for the later averaging that all pings together constitute a pingset are aligned, or else the averaging of the pingset could give ambiguous results. Echo alignment typically relies on tracking and indexing a temporal feature. The echoes within the pingset are then shifted in time to line up on that feature.

Hamilton proposed, when trying to extract the bottom echo, to first locate the sample of the highest level (S_v) of each ping and later use this sample as reference for the alignment [1]. Even though this method is easy to implement, the method is not error–free. Hamilton emphasized the problem of noise–peaks in the signal, which have the potential of creating false estimations of the maximum peak. However, for the data processed in this report the bandwidth of the different frequency channels are small. This prevents noise peaks and ensures all data received are smooth. In contrast with the sources that Hamilton saw as potential errors, the method of Hamilton itself was found giving errors. When locating the maximum peak of the total ping, which corresponds to the maximum peak of the first received echo from the sea bottom, fluctuations can occur. First of all the sampling interval can be a problem. If the sampling interval is too large, there is a probability that the first received echo not is sampled with enough

samples to ensure the *actual* maximum peak is located. Then a sample for example on the slope is determined maximum, a value that can be several dB lower than the *actual* peak. It is important to remember the acoustic equipment most often is designed for other applications than sea floor characterization, and therefore has limitations that must be considered. Another problem of locating the maximum peak is the effect of multiple reflections, which will be discussed in more detail later. This effect can cause constructive or destructive interference, masking the *actual* maximum peak. The last problem is the fact that no real data acquisition is error–free and there is a possibility of fluctuations caused by the equipment or other more natural causes as aeration. However, this last source of error is always present and is not particular for any specific method.

Instead of using the maximum peak for alignment, a threshold alignment method could be used instead. This method has shown to give better results for envelope alignment than the maximum peak method [11].

The threshold method exploits the consistency of the rising edge of the first received bottom echo for (almost) every ping, and was favored for alignment in this report. The next paragraphs explain the method step by step as it was implemented in Matlab. However, the basics should be the same regardless of which preferred digital processing tool being used.

The steps are as follows, with an illustrative representation of each step in figure 28 on page 43:

1. The first step is to locate the bottom echo. This step share in many ways Hamilton's approach with his way of locating the maximum peak of each ping. When locating the maximum peak of the ping – to avoid ringing effects from the transducer, the search for maximum peak must be started after a certain time delay. Two times the pulse length of the transmitted pulse were found satisfying. After the maximum peak is located, steps are taken in the backwards direction from the sample of the estimated maximum peak, to the sample where the level has fallen under a specific threshold value. The threshold value was determined by observation of the total pingset to be processed, to ensure the value was large enough. A large enough value is a value that lies on the rising slope of the first bottom detection of all pings, as indicated in figure 28. There is however a trade–off. The value should also be as small as possible ensuring a most precisely estimate of bottom depth and include as much as possible of the first echo.

2. The next step is to find the exact position of the threshold value. Often the value lies somewhere between two samples, and this must be corrected for. To ensure a sample at the position of the threshold value, interpolation can be used for re–sampling with an interval corresponding to the difference in x–axis value (either time or depth), between the sample just below the threshold value and the threshold value itself. As indicated on the figure's x–axis, this interpolation leads to different amount of samples of the sea floor echoes.

3. The last step is to compensate for the interpolation that was needed in the previous step. Then the signals are re–sampled back to a reference depth of the pingset – found as average pingset depth. This ensures every ping of the pingset has the same amount of samples and the depth dependency between each ping is compensated for. The results are illustrated in the figure.

Even if the threshold alignment method was found suitable for the task covered in this report, it should not be used without considerations. Sternlicht and de Moustier [11] emphasis that in high–noise environments or when signal shapes are highly variable the threshold alignment method may be ineffectual. They proposed another solution for this situation which can be found in their cited article.

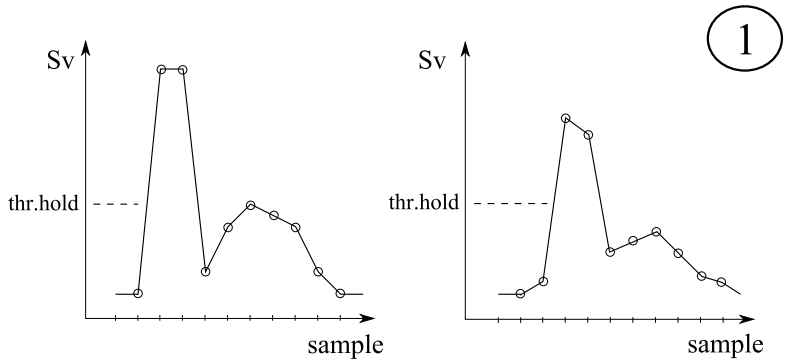

(a) Locate bottom echo by maximum peak detection and locating threshold level. Same amount of samples for all pings in each pingset.

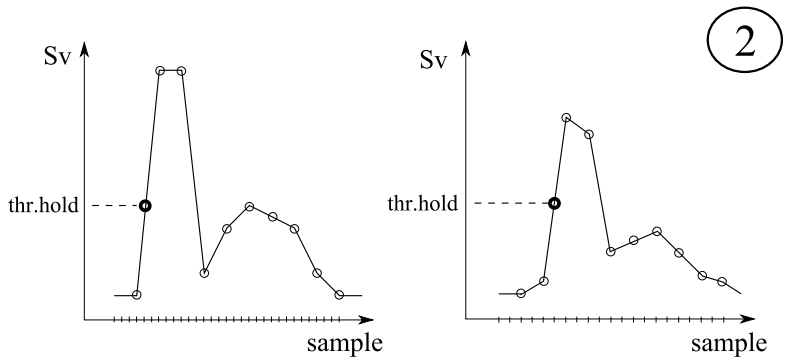

(b) Re–sampling to locate exact time/depth of threshold. Reject all samples before threshold. Different amount of samples between pings in each pingset.

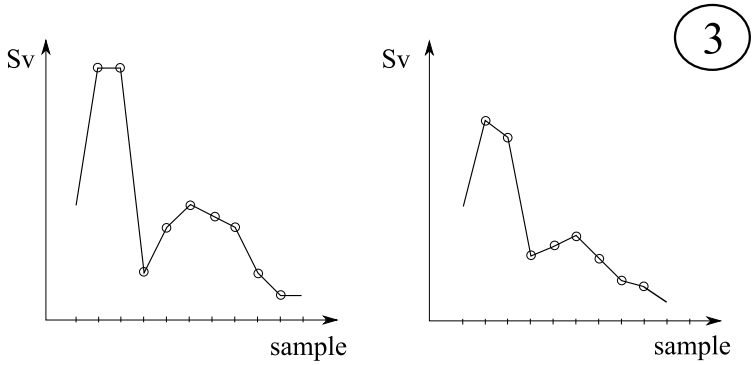

(c) Re–sampling to reference depth found as average depth of each pingset. Same amount of samples for all pings in each pingset.

Figure 28: Procedure for bottom pick. Example of two different echo shapes for each step.

4.2 Averaging and smoothing

After the first received echo from the sea floor is extracted from each ping and the threshold alignment method is applied to make sure every ping is aligned the same way, averaging of a selection of pings together forming a pingset is utilized. This averaging is done to suppress abnormalities as for example noise peaks and ping to ping fluctuations. The amount of pings to average needs to be large enough to get rid of the factors just mentioned, but not too large the level of detail decreases. In this report an amount of eight pings formed each pingset and were averaged. Eight were used based on observation and experience. Eight pings correspond to approximately $2m$ of vessel movement, calculated from a random SMASSC survey *.raw*–file by the $ER60$ software (will change for different vessel speed). The averaging technique applied can be found in equation 39 on page 24.

After averaging every pingset, additional smoothing is performed to reduce noise even further. A three point weighted average technique found in equation 40 on page 24 was used.

Figure 29 gives an example of pingsets after averaging and smoothing. In figure 29 (a) every eight unprocessed ping in a range of total 1000 consecutive pings were plotted. In this plot, fluctuations between pings can be easily observed. After performing threshold alignment and averaging of pingsets of eight pings followed by additional smoothing, the result became as plotted in figure 29 (b). The fluctuations are reduced and the echoes are more stable. The total number of pingsets in 29 (b) is actually not 1000 as indicated in the figure, but the floor value of 1000/8.

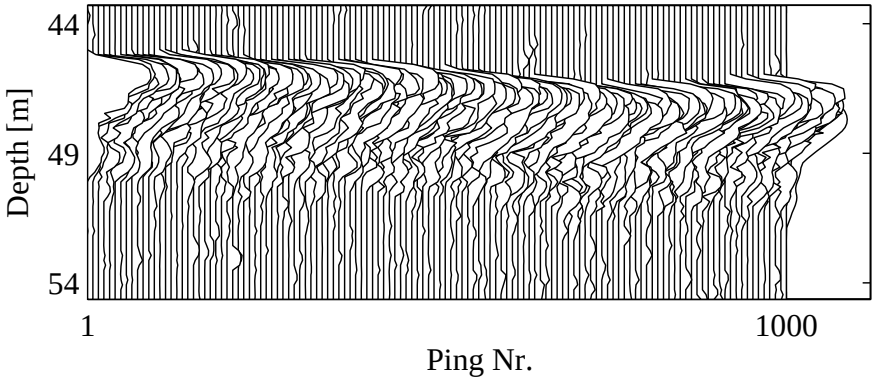

(a) Unprocessed bottom echoes

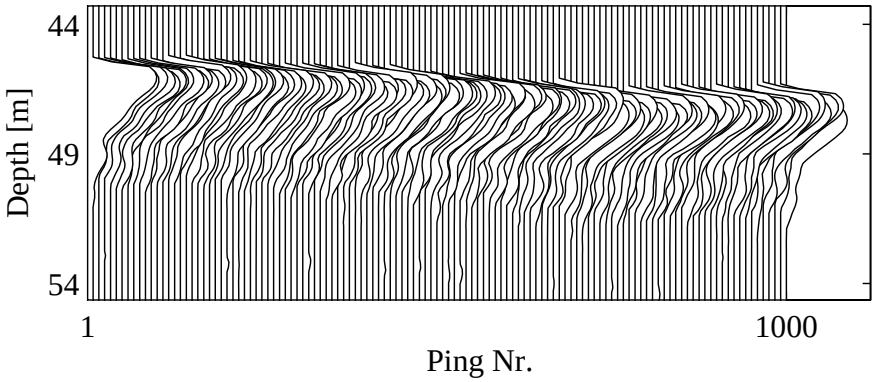

(b) Averaged and smoothed bottom echoes

Figure 29: Bottom echoes before and after threshold alignment, averaging and smoothing. Echo amplitudes are Sv values. The frequency is $18kHz$.

4.3 Reference depth

The last main approach in the signal processing, before performing the variable analysis, is to correct for depth dependency between different averaged *pingsets*. The theory behind the correction can be found in 2.3 on page 21.

In the theory for power corrections, a TVG function is proposed used when compensating for amplitude loss as a result of spherical spreading and absorption. This TVG function has not explicitly been implemented as a separate procedure for this report, when finding the Sv values implies compensation for spherical spreading and absorption. These Sv values are output parameters from the *.raw*–reader provided by IMR, which means the data provided already has a TVG function applied to it. Should however one wish to use unprocessed power values, a TVG function should be applied before further processing or analyzations of the data.

Time correction involves compensation for different time–duration of echoes as a result of different depths where the echoes are collected. The principle is explained in 2.3.

Implementation of time correction is in many ways the same as how different echoes of a pingset were processed before averaging. There might be several approaches, but only the approach implemented for this report will be explained.

Time correction involves first to find a reference bottom depth, which can be taken to be the average bottom depth of all pings to be processed. The same depth must be used for all pings involved in the processing. Then a new interval between each sample can be computed for all averaged pingsets, based on the factor between the bottom depth of each pingset and the average bottom depth. Interpolation is then used for re–sampling, to make sure that all bottom echoes with the same type of bottom properties now have the same amount of samples and no longer are elongated or compressed respective to each other.

4.4 Echo variable analysis

In the next section, how the different variables calculated from the processed echoes are described. Only what thought as the most important variables for describing the echoes are presented.

4.4.1 Peak value

The Sv value of the highest peak of the first received echo.

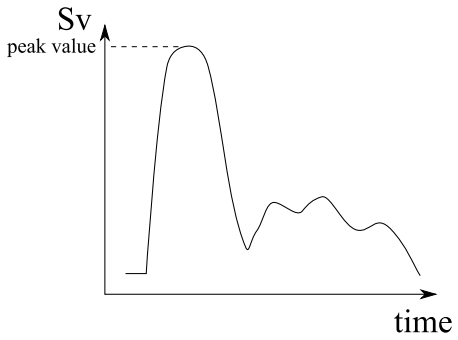

Figure 30: Peak value

4.4.2 Rise–time

The rise–time is defined as the time it takes the echo level to reach a fixed maximum threshold value from a fixed minimum value. The maximum threshold value should be some dB lower than the maximum peak level, $10dB$ lower than peak level were used in this report. The minimum threshold level were defined as the fixed start level of the processed pingsets, in another word the first sample value of every pingset. This value is global for all processed pingsets.

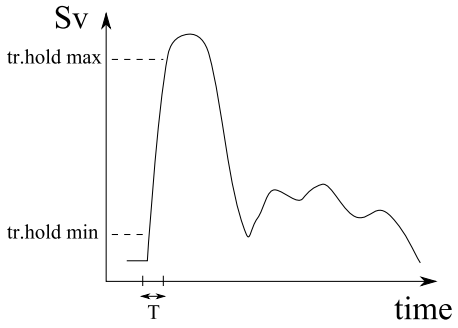

Figure 31: Rise–time

4.4.3 Fall–time

The fall–time is defined as the time it takes the echo level to decrease to a fixed minimum threshold value from a fixed maximum value. The maximum threshold value should be some dB lower than the maximum peak level, $10dB$ lower than peak level were used in this report. The minimum threshold level were chosen analytically, but should lie somewhere on the falling slope from the maximum peak. $30dB$ below the maximum peak were chosen in this report.

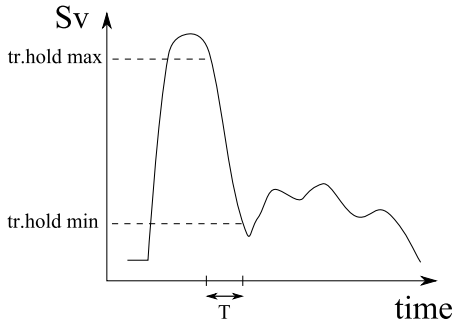

Figure 32: Fall–time

4.4.4 τ – 10dB, 20dB, 30dB, 40dB and 50dB

τ is defined as the time–interval between the two points on either side of the main peak, where the level has fallen respectively $10dB$, $20dB$, $30dB$, $40dB$ and $50dB$. If the start level of a ping exceeds one of the values, the global start value for all processed pings should be used for every pingset.

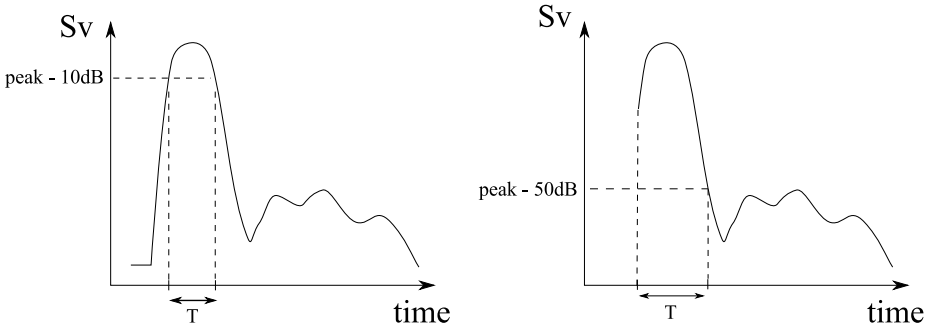

Figure 33: τ – $10dB$ and $50dB$

4.4.5 Slope of tail

The slope of the tail is the estimated slope from an optimized line between averaged intervals of Sv values of the echo tail. The tail is defined as all samples after the level has fallen a certain dB value from the maximum peak, plus a delay of N–times the pulse length. In this report $40dB$ below the peak value were used as threshold.

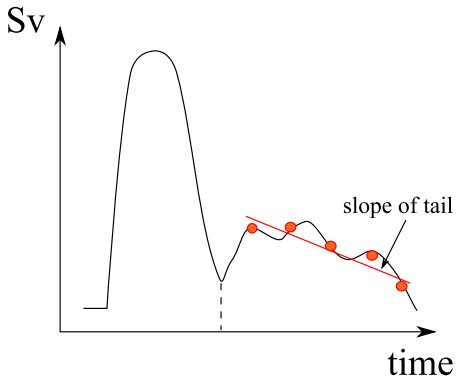

Figure 34: Slope of tail

4.4.6 Ping area

The area of the received echo is probably the most informative parameter. Since there are large differences in level values of each ping, the area is calculated as dBm and not in the linear domain. dB times meter, dBm, is an un–physical quantity, but is used to be able to extract parts of the signal that in a linear scale would be negligible. Both the total area of each ping and the area of the tail are calculated. The tail is defined as all samples after the level has fallen a certain dB value from the maximum peak, plus a delay of N–times the pulse length. In this report $30dB$ below the peak value were used as threshold.

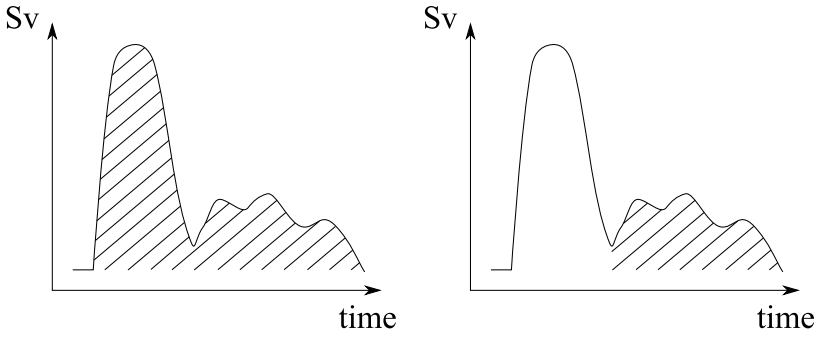

Figure 35: Area of total ping and tail in dBm

5 Possible sources of error

5.1 Sloping seabed and ship roll/pitch

When the seabed has a sloping profile, the illuminated area by the echosounder beam will differ in shape and size compared to the situation of a perfectly horizontal seabed. Scattering properties and received echo of a sloping bottom (assumed being rough) are illustrated in figure 36.

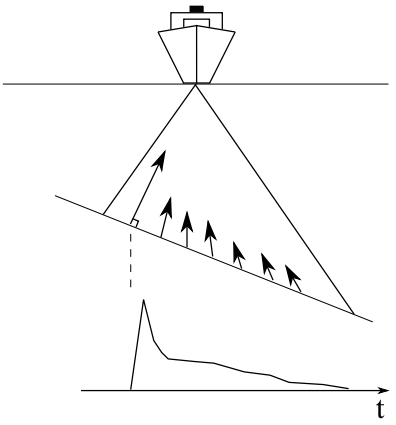

Figure 36: Echo properties of a sloping seabed.

A seabed slope can both lengthen and distort the received echo. Also, the specular reflection will not be reflected from the acoustic axis, therefore masking the true depth for sloping bottoms. If the slope is steeper than half the beamwidth, the specular reflection will not be received at all.

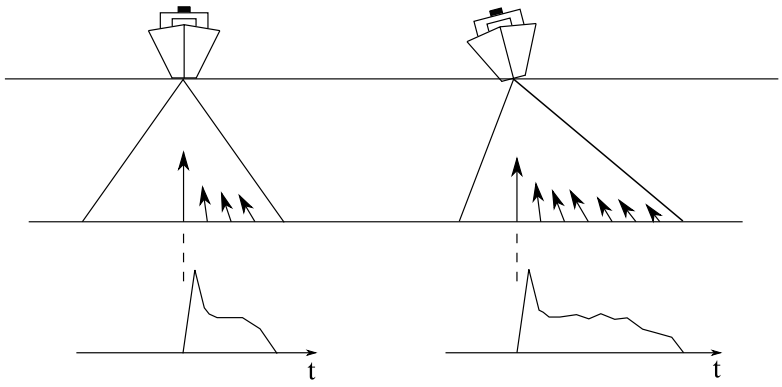

Figure 37: Echo properties of no ship roll and with ship roll.

Another situation that in many ways share the same possible problems as a sloping bottom can cause, is ship roll or pitch. Especially in rough seas the ship roll and pitch

can become important. Many newer sonars do compensate for both roll and pitch by physically stabilizing systems, but normal echosounders do seldom have such systems. A situation of ship roll is illustrated in figure 37.

Ship roll and pitch do as a sloping bottom, lengthen and distort the received echo. However, the specular reflected wave will represent the correct depth regardless of different ship roll or pitch – as long as the roll or pitch is less than half the beamwidth and the sea floor has no sloping profile.

In this project, only almost perfectly horizontal sea floors were studied to avoid the sloping effects. Ship roll and pitch were not compensated for, but were never larger than half the beamwidth for any of the data processed.

5.2 Multiple reflections

There is definitely not always an easy task to extract the bottom echo and make global assumptions on behalf of what received. Even if the bottom sediments are homogeneous over a certain area, large fluctuations on ping to ping basis in echo shape do often occur. These fluctuations are minimized by averaging, but can be of a such scale that the averaging will be highly affected by the fluctuating pings of each pingset.

Multiple reflections is a problem that can cause large fluctuations in the received echo shape. This effect do most often occur when the shape of the sea floor changes within an area illuminated by the acoustic beam during a ping. The changes can be caused by rocks or other large objects lying on or half buried in the sea floor. Multiple reflections constitute among other factors a possible problem for the threshold alignment method which was used for this report, and was described in 4.1 on page 40. The multiple reflections effect is illustrated in figure 38.

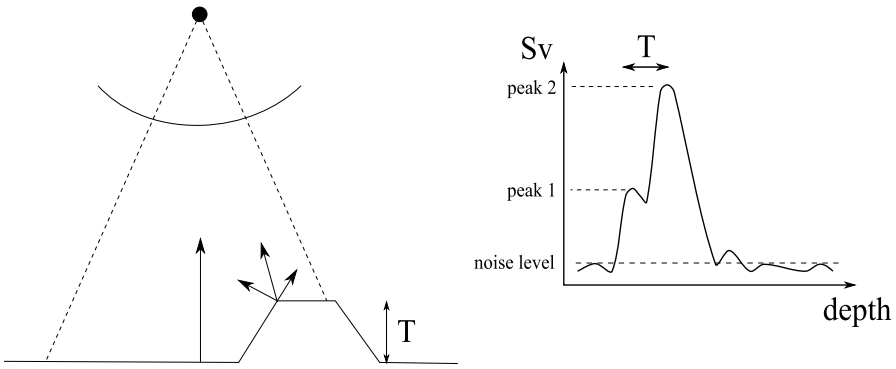

Figure 38: Multiple reflections. Sea floor is assumed perfectly hard.

In the figure the transmitted wave, which is assumed having a gaussian shape in the time domain, will first hit the shallowest point on the illuminated part of the sea floor. Because of the irregularities at this point, the wave will be scattered in different directions. Some of the energy will be backscattered, causing the first peak on the graph to the right. At time T after first impact with the sea floor, the wave will hit the area perpendicular to the horizontal part of the sea floor – straight below the source/receiver. Since this area is totally flat, all the wave's energy at this point will be backscattered, causing the highest peak in the graph. The contributions from the different parts of the sea floor can in addition interfere, causing constructive or destructive interference patterns.

An example from real data of fluctuations in bottom heights causing multiple reflections is given in figure 39 on the next page.

In the figure the bottom heights of area one and two are about half a meter and both areas contain approximately 70 pings. Examples of affected bottom echoes from the two areas, can be found in figures 40 on page 54 to 43 on page 55. Figure 40 and 41 on the

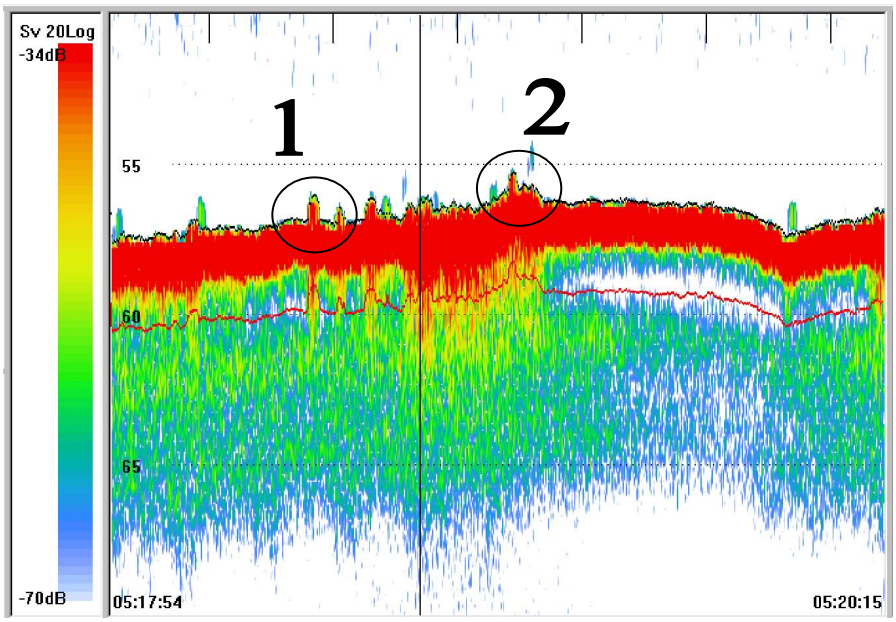

Figure 39: Fluctuations in bottom heights causing the multiple reflections effect.

following page are from the first area while figure 42 and 43 on page 55 are from the second. The blue graph in each of the figures has been affected by multiple reflections, while the gray shaded graph is an example of a bottom echo from the same area that is not affected by multiple reflections. The frequency of the acoustical signal is for all graphs $18kHz$.

There is possible to observe the first reflection from the shallowest part of the illuminated sea floor in all figures, as explained in the theoretical model of figure 38 on the facing page. The reason why figure 41 and figure 43 has a smaller maximum peak level than respectively figure 40 and figure 42, are because these bottom reflections are taken from pings closer to the irregularities of area one and two in the echogram. In another word these figures are from pings where more of the irregularities are covered by the beam. Since the irregularities probably are objects of greater roughness as for example rocks, some of the wave's energy at normal incidence will be scattered in other directions. A reason for the fluctuation around the maximum peak can be interference patterns from the different scattering directions. When changing the frequency of the acoustic signal, the multiple reflections effect will still be a problem. For higher frequencies, the beam–width will decrease, but as long as the irregularities are within the illuminated part of the sea floor, multiple reflections can occur.

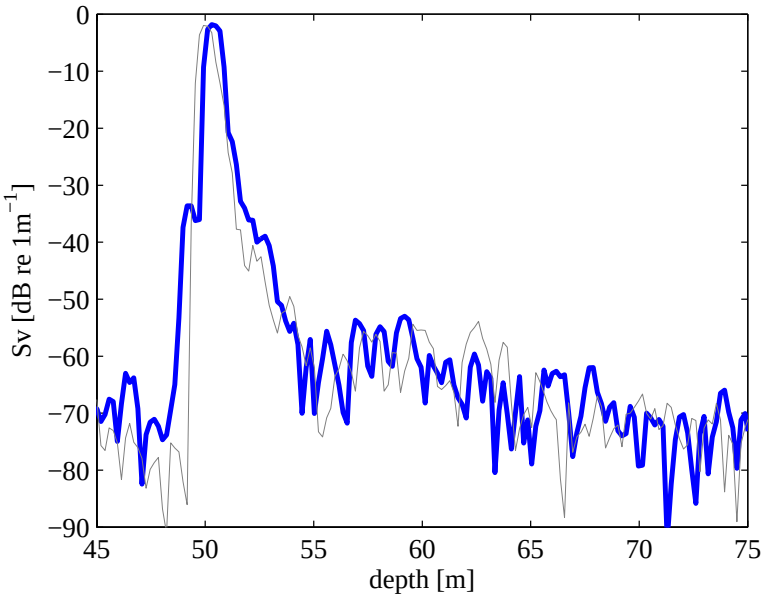

Figure 40: Bottom echoes from area 1 (RAW)

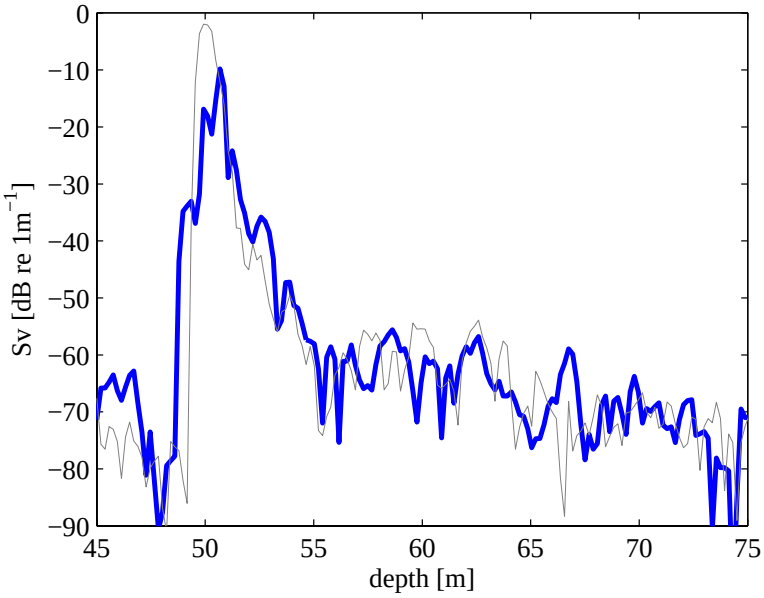

Figure 41: Bottom echoes from area 1 (RAW)

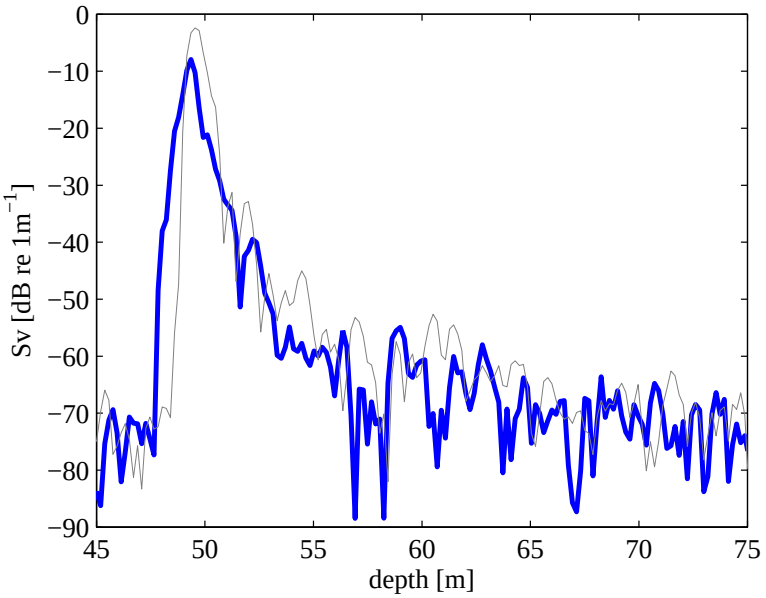

Figure 42: Bottom echoes from area 2 (RAW)

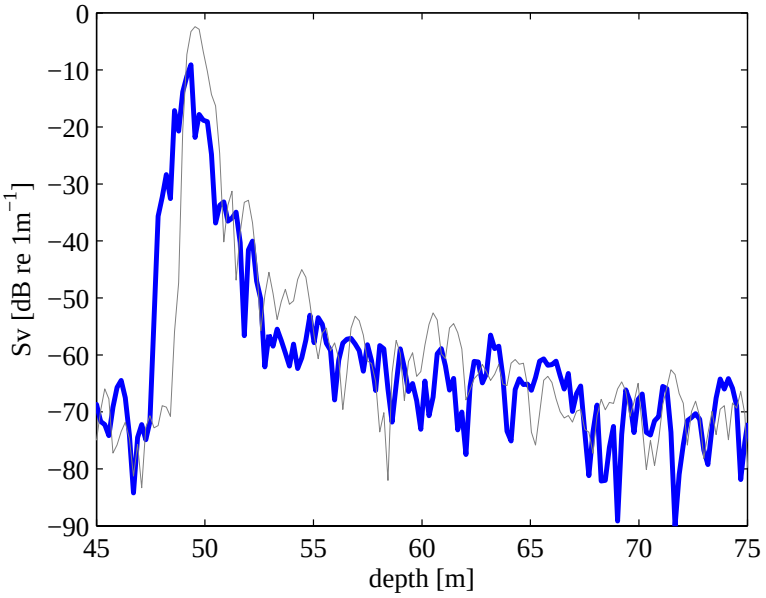

Figure 43: Bottom echoes from area 2 (RAW)

6 Echo parameter analysis and discussions

6.1 Introduction

The next section will present results from the variable analysis performed on data collected during the SMASSC 2008 survey, for selected parts of the sea floor. All methods used to measure the variables were described in 4.4. The main goal of the section is to distinguish different sea floor parameters based on the variable analysis, and try to elucidate whether or not these parameters can be used to find typical sandeel grounds. Therefore, only what *thought* as relevant parts of the sea floor are considered – going through the data from the whole survey would be too time consuming considering the time limits of this project.

To systematize the representation of data and discussions, first two selected parts of the sea floor with different observed echogram will be presented and compared. All variables calculated from processed received bottom echoes from both regions of the sea floor were found, but will be given different attention based on both consistency between calculated variables of each region and differences observed between the regions. The different variables will mostly be presented and discussed separately as a matter of form, even though this is somewhat a bit unfortunate considering many of the variables are highly connected to each other. Echogram of the two parts of the sea floor for the $200kHz$–channel can be found in figure 44.

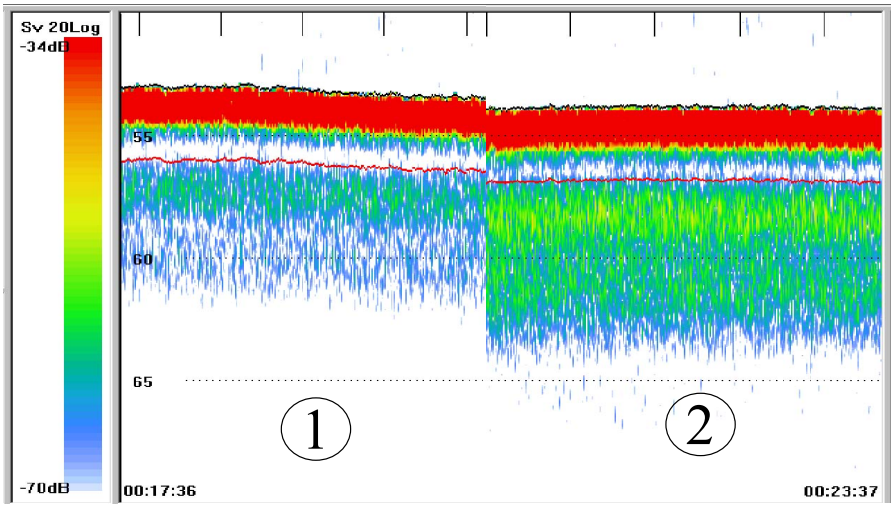

Figure 44: Echogram of two spatially separated sea floor regions. Region number two is possible sandeel area. The frequency is $200kHz$.

In the echogram, region two corresponds to the region with largest sledge catch–size during nighttime from the SMASSC survey, presented in the SEABEC results (3.3). Therefore, there is a probability this region corresponds to typical sandeel grounds. Re-

gion number one was chosen because of its close location to region number two – the distance between the two regions was approximately 250 meters based on the vessel's distance of movement (vessel assumed following a straight path). A smooth transition could be observed from the echogram between the two regions and there is a possibility many of the sediment properties are equal for both regions, even if the echogram *looks* different at $200kHz$. Since the bottom type is unknown, this nearness can be an advantage if sandeel catch–size is assumed being much smaller of region one compared to region two. Then possible differences between different estimated parameters of the echoes could tell what parameters and the parameters' "frequency response" that are important, for the sea floor being a possible sandeel ground.

After the two sea floors have been compared for different parameters, more examples from different sea floor regions will be given and discussed. The location of these examples will be given as they are presented.

In the discussions, when referring to different parts of the bottom echo, different expressions describing the echo will be used – and must be clarified in advance. The first received part of the bottom echo, most often corresponding to the specular reflected wave, will be expressed as the main part of the echo. The subsequent part will be expressed as the echo tail.

6.2 Comparison of two regions of the sea floor

6.2.1 Total echo area

In figure 45, ratios between frequencies of total bottom echo area for the two spatially separated regions of the sea floor are plotted. Echogram of the two regions can be found in figure 44 on page 56. In the figure, region one is plotted with a blue color while region two is plotted with a red color.

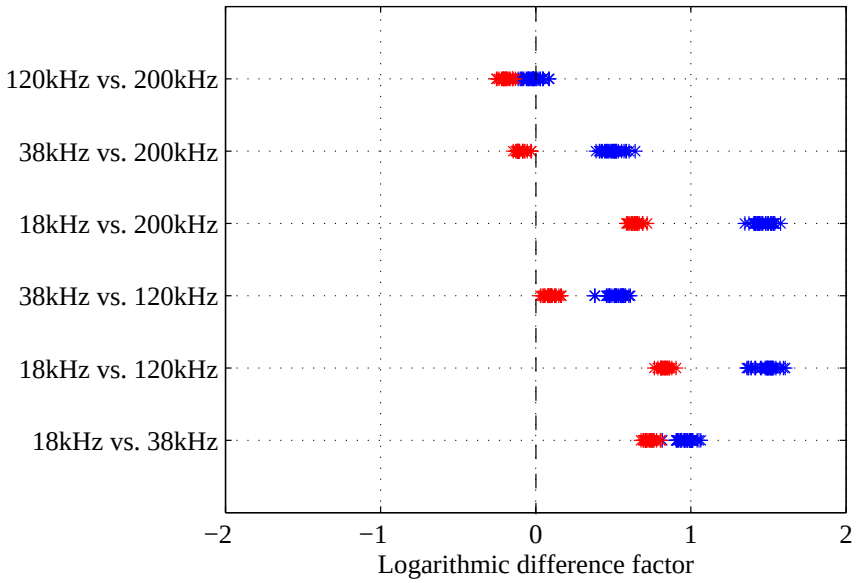

Figure 45: Total echo area ratios between different frequencies. Blue: Region one. Red: Region two.

For every parameter in figure 45, 30 consecutive averaged pingsets are plotted for each sea floor region to emphasise consistency between pingsets. Be aware that the difference factor, or the ratio, is in logarithmic units. The closer each ratio is to zero, the more equal the echo areas between the frequencies are. All processing were performed as described in 4.4.6 on page 49, to calculate the area of each echo in dBm at every frequency.

When looking at the plots in figure 45 of the frequency ratios, the first observation is that there definitively *are* some differences between the ratios of the two regions. This contention is solely based on the consistency of the plots for each area and separation of the plots between the two regions. How large the differences are between the two regions and what sea floor properties that cause the differences, need a more in depth consideration.

The differences in each frequency ratio can indicate possible bottom properties of the two regions. The easiest start is to compare the two regions to each other, before trying to extract specific individual property information. For all frequency ratios, the difference

factor measured for region two are generally smaller than the ones measured for region one – which indicate less difference in echo area between the frequencies of region two compared to region one. Especially the ratios concerning the highest frequencies versus the smallest show great decrease in the difference factor. It might be easier to observe these differences from plots of measured echo area for each single frequency for the two sea floor regions – therefore these results have been plotted in figure 46. All parameters were the same when plotting figure 45 and 46. The solid lines of the plots indicate calculated mean values. In figure 46, the change between the two regions is small for the $18kHz$– and $38kHz$–channel. In fact, for the $18kHz$–channel, the echo areas are so close they can be considered as being the same. This indicates the main change in sea floor properties between the two regions, mainly affect higher frequencies (compared to what measured in this report).

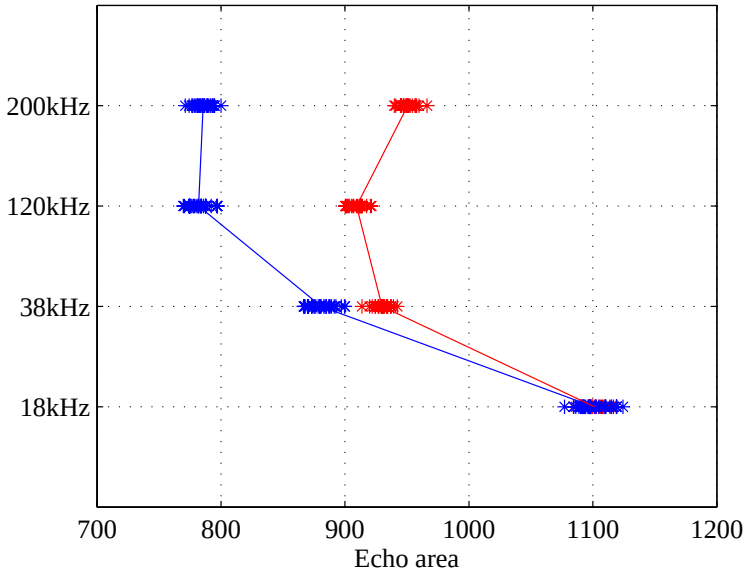

Figure 46: Total echo area for single frequencies (dBm). The threshold minimum from where the area was calculated was $-120dB$. Blue: Area one. Red: Area two.

To be able to analyse figure 46, one must know what sea floor properties that affect the echo area of the high frequency–channels. Since the frequency is high, variation in the roughness relief will highly affect the echo–shape. Bottom sediment scattering will most likely not be affecting the signal shape much at high frequencies, especially when no variation for the $18kHz$–channel can be observed – the frequency most sensitive to changes in bottom hardness. Therefore properties of the interface are assumed being the main factors. As stated in the theory section, emphasized in figure 12 on page 17, increased roughness relief heights make the scattering more diffuse. More diffuse scattering increases the scattering strength from oblique angles, causing a more prominent tail of the echo. Even though the specular reflection decreases for a more rough sea floor, the tail will most probably dominate, causing an increased echo area of the total

received echo for larger roughness relief heights.

Back to figure 45 and 46; as can be observed, all ratios between the highest and lowest frequencies decay more for region two compared to region one in figure 45. In addition, the frequencies $120kHz$ and $200kHz$ do decrease considerably more than the other smaller frequencies in figure 46. This indicates, when following the previous paragraph's elucidation, the roughness of area two are greater than the roughness of area one. Also, this increased roughness is small–scaled, when none of the other (smaller) frequencies were affected. Considering the sledge–samples, SEABEC results and possible sandeel habitat choice of a more coarse sediment, area two would compared to area one single out as a more preferred sandeel ground based on the bottom echo area differences for the high frequency–channels. This can off coarse not be stated as an absolute truth when type of bottom is unknown, but shows the potential that lies in echo area calculation of the received echo. Had sea floor one been for example fine–particled sand, sea floor two would have shown typical behavior of being coarser graveled sand based on the previous assumptions.

The shape of the echo area "frequency response" of figure 46 is interesting. Considering the differences between the two sea floor regions, the shape of region two might indicate a possible general "frequency response" that stays the same for a later encountered sea floor with many of the same properties. This must however be investigated further and is just a hypothesis at this point.

There were not found any major differences between calculated total echo area and calculated area of the echo tail.

6.2.2 Echo fall–time

Figure 47 shows plots of measured echo fall–time for the two regions of the sea floor. The fall–times were found as described in 4.4.3.

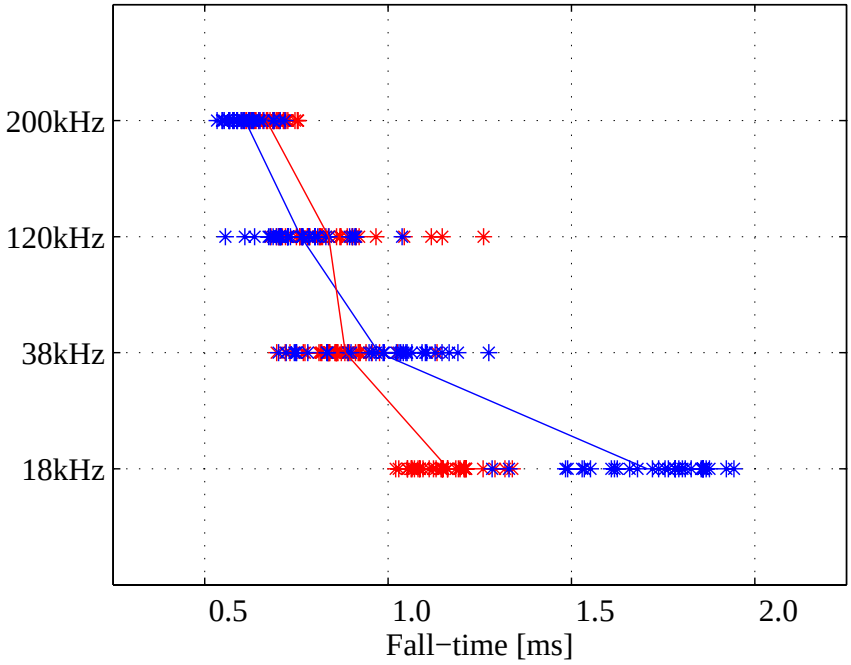

Figure 47: Frequency differences in measured echo fall–time. Blue: Region one. Red: Region two.

As can be observed from the figure, the calculated fall–time values are more separated and not as consistent as for the echo area. This indicates the fall–time variable is more dependent on fluctuations between consecutive pings. However, there is still possible to extract some useful information from the figure.

First of all, and most important, one can observe a greater difference between calculated fall–times for the $18kHz$–channel than all the other channels. In fact, the values for the two regions of the other channels are so close, they must be assumed being the same when analysis solely is based on observation. Anyhow, a difference in fall–time for the $18kHz$–channel can indicate a difference in sea floor hardness between the two regions. For a perfectly hard and flat sea floor, one would expect the shape of the received echo pulse as being very close to the shape sent from the source. Then the fall–time would be the same between different parts of the sea floor. Further, since the echo at the $18kHz$–channel not will be altered in a great extent when the sea floor has small–scaled roughness, as the discussion for the echo area results suggested in the previous section, the roughness will probably not alter the echo shape – causing different fall–times. As a

result the hardness difference is most probably the reason for different fall–times between the regions.

Since the fall–time of region one for the $18kHz$–channel is larger than the fall–time of region two, region one most probably consists of a softer bottom type than region two. A softer bottom will increase the width of the received echo for smaller frequencies, when additional sediment scattering increases for a softer sediment. The sediment scattering will only contribute to the total scattering strength after a time interval, when the dominating surface scattering has decreased to a certain level. Therefore the fall–time becomes larger for a softer sediment.

The assumption that region two consists of a harder bottom, is also in accordance with the fact that a rougher bottom typically is harder than a softer. This was also the result of the last section (6.2.1). However, difference in hardness can not be observed from the last section, when the total echo measured for $18kHz$ are the same for the two regions. There is not enough sensitivity in the total echo area. In addition, fluctuations between pingsets could contribute in the same extent as the extra sediment scattering, to the total measured echo area.

6.2.3 Echo rise–time

When calculating the rise–time of the echoes, no specific differences were found between echoes for different parts of the sea floor. This is mainly caused by the fact only horizontal and almost flat sea floors were studied, and the rise–time is then mostly dependent upon the electronic equipment used. Both the signal shape and limitations in the sampling frequency will determine the rise–time.

However, the rise–time could indicate whether the sea floor has fluctuating reliefs causing multiple–scattering effects. The situation of multiple reflections were explained in 5.2.

The rise–time parameter will not be studied any further in this report.

6.2.4 τ – 10dB, 20dB, 30dB, 40dB and 50dB

In figure 48 on the next page, calculated mean values of τ for different dB–values below the main peak are plotted for different frequencies. τ was defined as the time interval between both sides of the main peak where the level had fallen a certain dB–value. Figure 48 (a) is from region one while 48 (b) is from region two. The reason only mean values are plotted, is because of the closeness and to some extent overlapping values between the different frequencies of the regions. Standard deviations could be included, but were considered giving poorer information value and were therefore excluded from the plots.

The consistency between averaged pingsets was found poorer the more the level had fallen from the maximum peak, which also is expected since the major influence of scattering caused by interface roughness and sediment properties then will become more important.

The different τ values can give a good indication of the shape of the received main echo pulse. In many ways the different τ values can be seen as more detailed versions of the fall–time, since the rise–time stays more or less the same for a sea floor without large fluctuations in roughness reliefs – though their magnitudes will off coarse not be the same.

When comparing figure 48 (a) and 48 (b), an observation is the plots from region one are more separated than the plots from region two. In another word the differences of τ, or width of the main echo pulse, are larger between the frequencies in region one. Especially the $18kHz$–channel marks out as different in region one, with a much higher value of τ. This can indicate, as for the fall–time of section 6.2.2, the sea floor is more soft. When considering sea floor two, where the difference between the frequencies are considerably smaller, the plots can indicate the sea floor is more hard.

When the echo level has fallen $50dB$ from the maximum peak, τ could give an indication of roughness properties. As for region two, τ becomes much larger for the highest frequencies ($18kHz$ and $200kHz$) which can indicate larger roughness of this area. In contrast, τ of the highest frequency in region one do not show any major increase. However, for the $120kHz$–channel the increase is prominent for region one, which is somewhat misleading considering the findings of the previous sections – and can indicate uncertainties in τ. Especially values calculated far from the maximum peak are vulnerable of echo fluctuations and might show poor consistency on a pingset to pingset basis.

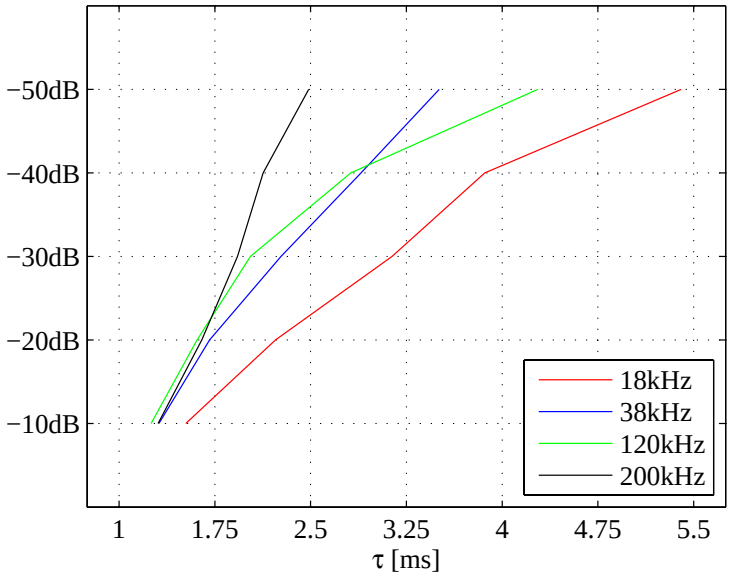

(a) Region one

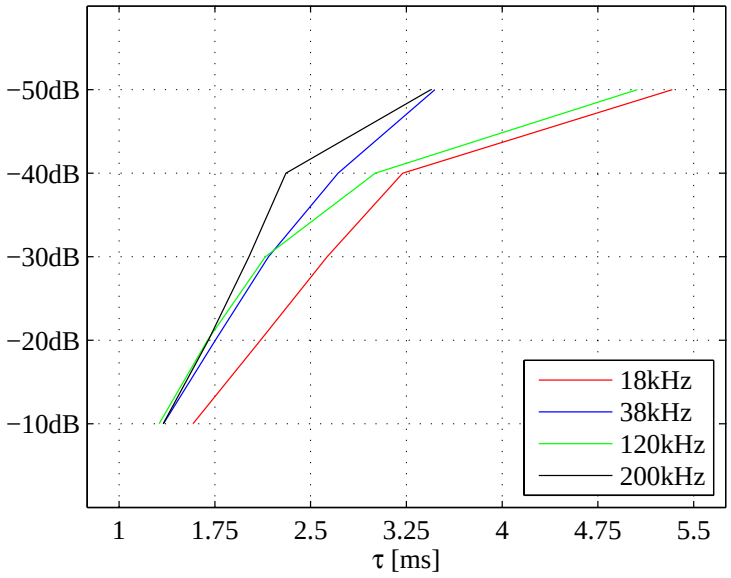

(b) Region two

Figure 48: τ effective for different dB–values below maximum echo peak, for the two regions of the sea floor. The plots represent calculated mean values.

6.2.5 Slope of echo tail

In figure 49 (a) and 49 (b), examples of how the slope of the echo tail is found can be seen for two different frequency channels. The plots were taken directly from the calculation routines and are therefore showing exactly how the slopes are calculated. The solid straight line represents the optimized line between the five averaged points of each small interval of the tail, where the slope of the line gives the slope of the echo tail.

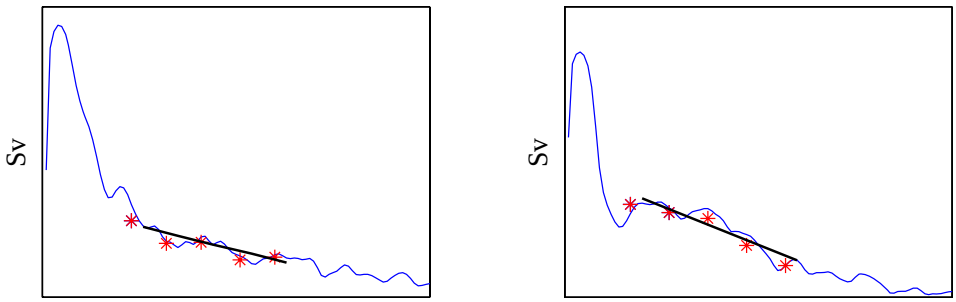

(a) $18kHz$ (b) $200kHz$

Figure 49: Examples of how the slope of the echo tail is found. The examples are taken directly from the calculation routines.

The calculated slopes of the echo tail for different frequencies of the two sea floor regions can be found in figure 50. Be aware of the minus sign for the slopes, which indicate decreasing Sv values of the tails. The solid line between each frequency of each region represents the calculated mean value of the tail slope. In addition, standard deviations of the 30 pingsets calculated for each region at every frequency, show the consistency between values for each region.

As can be observed from figure 50, only calculated standard deviations for the slopes of the $200kHz$–channel are not overlapping between the two regions. This indicates a possible distinction in echo slopes between the regions for the $200kHz$–channel. For the other channels, the distinctions are not as clear – indicating some of the calculated slopes between the two regions probably are overlapping.

The slope of the echo tail can give an indication of the amount of scattering from oblique angles. When considered for the different frequencies, the slope can give information about both hardness and roughness properties of the sediment. A steep slope for the lowest frequencies can indicate a harder bottom, while a gentle slope a more soft bottom. This situation yields for small scaled roughness reliefs. The same situation can occur for large scale reliefs, where the scattering from oblique angles can be large even if the frequency is low. This is a trade–off, but can be supported by other variables, like τ or the fall–time, which determine the width of the main echo and not the tail. If then the width is found large for the main echo, there is a larger possibility the additional tail

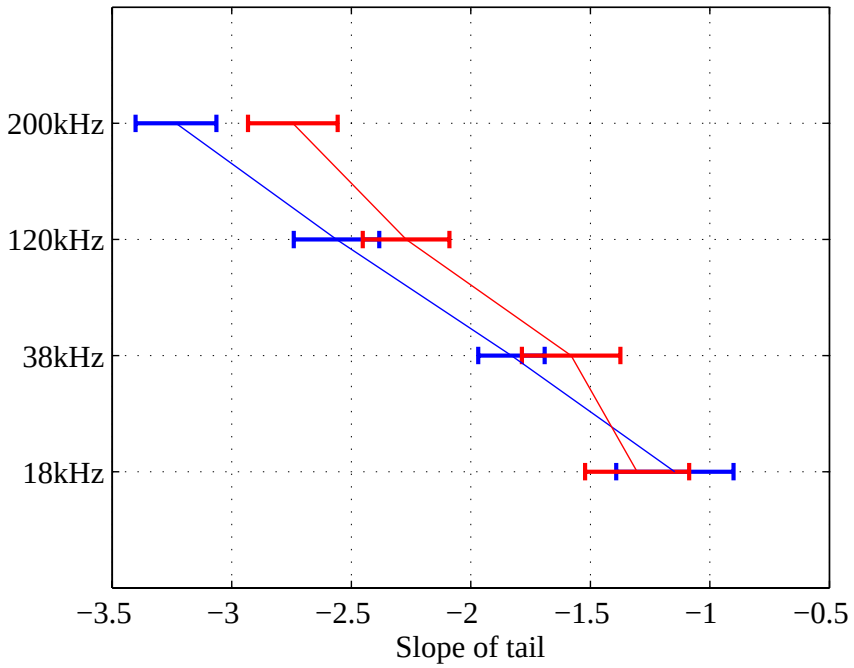

Figure 50: Calculated slope of echo tail for different frequencies. Blue: Region one. Red: Region two.

roughness is caused by a soft sediment. For higher frequencies, a steep tail slope most probably indicates less roughness than if the slope is gentle.

There is very important when calculating the slopes, where to define the tail. If the tail includes contributions from the main echo, the explanation in the previous paragraph might be wrong. This yields especially for the smaller frequencies, where the situation then might be the other way around.

For the situation treated in figure 50, since the slope is steeper for region one than for region two, region one has most probably less roughness than region two and could be favoured as a sandeel ground.

6.3 Comparison of four regions of the sea floor

In the next section, four different parts of the sea floor of "Vestbanken" will be studied. The motivation for picking these four different parts was based on the results from SEABEC and sledge samples. The four regions are listed below, where also additional information of the regions can be found.

Region 1

- Corresponds to region 1 in the SEABEC results from "Vestbanken", where the largest catch–size of sandeel was made.

Region 2

- Corresponds to region 2 in the SEABEC results from "Vestbanken", where the second largest catch–size of sandeel was made. The SEABEC results for this region differed from the results of region 1.

Region 3

- Corresponds to region 3 in the SEABEC results from "Vestbanken", where the fifth largest catch–size of sandeel was made. The SEABEC results for this region was close to the results of region 1.

Region 4

- No sandeels were found by sledge samples in this region during nighttime. The coordinates of this position was $[lat : 57.232, lon : 5.652]$ and can be found the SEABEC results of "Vestbanken" in figure 22 on page 34.

6.3.1 Total echo area

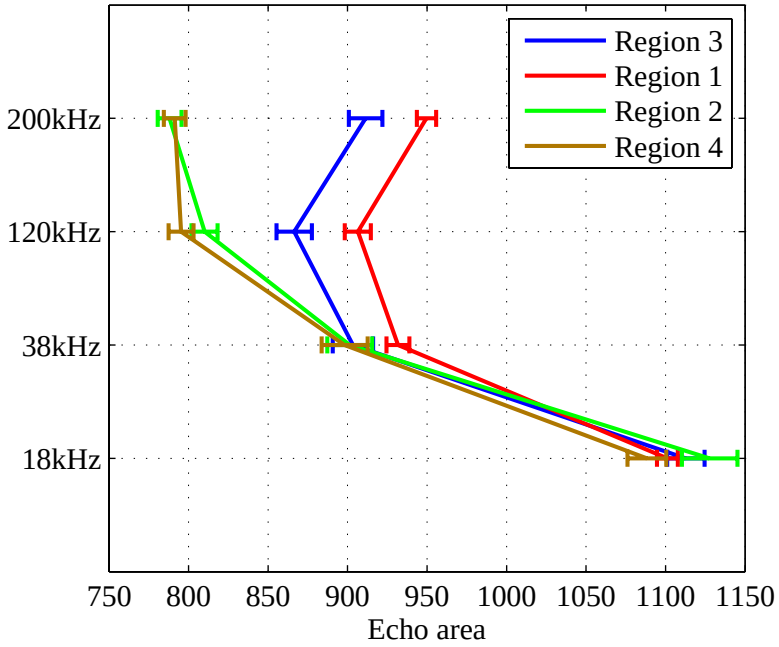

Figure 51: Total echo area for the four different parts of the sea floor, measured at different frequencies.

When comparing the total echo area of the different regions, one can observe the shape of the frequency responses of area one and three almost are the same. This yields also for region two and four, but which differ from the responses of region one and three. Considering region two had a quite large catch–size while region four had none, one would expected more separated values than figure 51 shows, if typical sandeel grounds were thought being constant. For region one and three, the bottom properties affecting the echo area can be considered being almost the same based on the similarities of their frequency response. Their frequency response can indicate a typical frequency response for sandeel grounds, but does not explain why the frequency response of region two is different. The difference indicates the properties of region two probably are different from region one and three. As a result, the similarities in sandeel catch–size may actually indicate the complex behavior of the species, more than a single typical sandeel ground.

6.3.2 Maximum peak

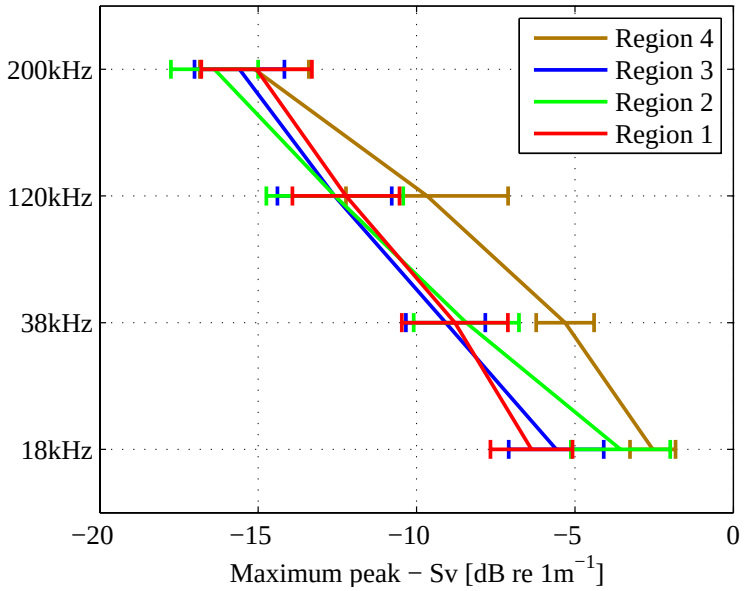

Figure 52: Maximum peak values for different frequencies, plotted for the different regions.

The echo peak values are generally fluctuating quite a lot, and can differ by several dB from ping to ping. Therefore it can be dangerous to make any conclusions based on these values. However, the peak values can give an indication of sea floor irregularities. A smooth and flat sea floor without any large differences in shape or sediment properties should give a more stable echo than a fluctuating sea floor. When averaging a set of pings, the averaged peak should then reflect this stability. This might be the situation in figure 52, where region four has higher peak values for the two lowest frequencies and has a better concentration of these values. This can indicate region four is smoother and more flat than the other regions.

6.3.3 τ – 10dB, 20dB, 30dB, 40dB and 50dB

In each of the plots in figure 53 the different regions are plotted for different values of τ. Each plot represents each of the frequency channels.

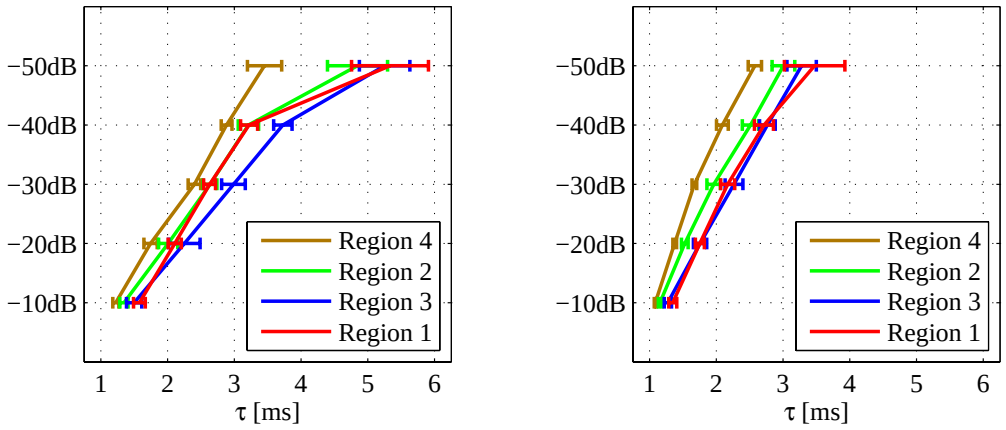

(a) $18kHz$

(b) $38kHz$

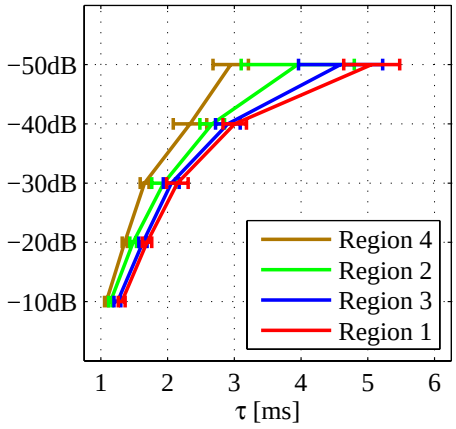

(c) $120kHz$

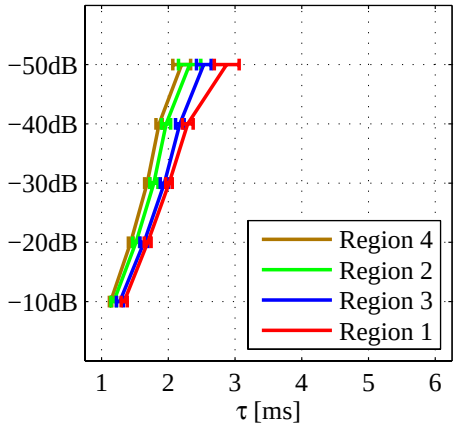

(d) $200kHz$

Figure 53: τ effective for different dB–values below maximum echo peak, for the four regions of the sea floor. Each plot represents the different frequency channels.

A trend for most plots of the figure are the separation between the regions, where τ values for region four are lowest, region one are highest and region two and three lie in between. The exceptions are for the $18kHz$– and the $38kHz$–channel, where different τ values get smaller for region one and deviate from the trend. The reason for this is hard to explain, but could indicate region three is consisting of a softer sediment than region one.

The reason region four has generally lower τ values, could be a result of generally higher

maximum amplitudes of the echoes of this region as indicated in the previous section. The program calculates the τ values based on how much the level has fallen from the maximum peak, and since additional roughness scattering and sediment scattering are most important when the specular reflection no longer is dominating, these additional scattering effects will not come into play when the maximum peak level is high. This situation is an error by the calculation routines, but is hard to compensate for. One should actually expect the τ values were higher for region four, considering this region most probably has less roughness and therefore most probably consists of a softer sediment than for example region one. For eliminating these assumptions, one should have carried out sediment samples that could tell the bottom type and roughness properties for the regions.

6.3.4 Echo fall–time

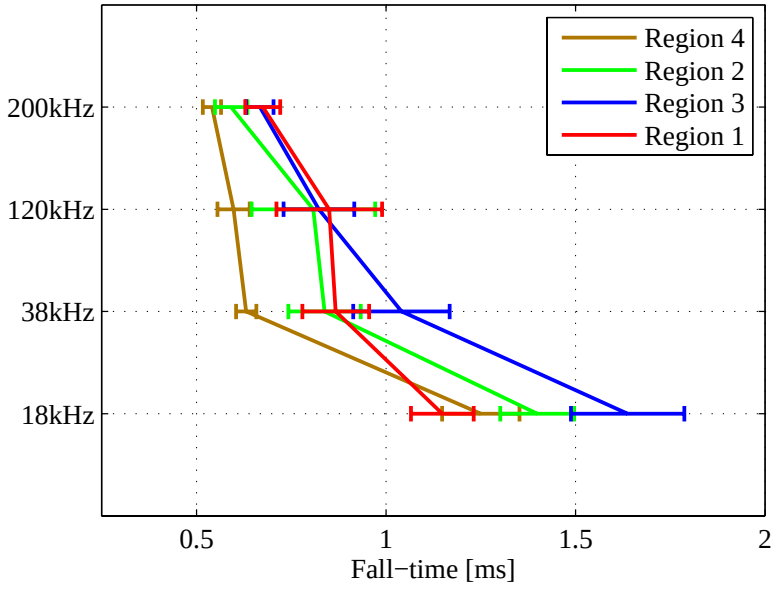

Figure 54: Fall–time for different frequencies, plotted for the different regions.

The echo fall–time of each region, as plotted in figure 54, indicates region three consists of a softer sediment than the other regions based on the higher fall–time values at $18kHz$ and $38kHz$. On the other hand, region four shows indication of being smoother (more flat) and probably more hard as a result of generally lower fall–time values. However, as explained in 6.3.3, this might be a result of higher maximum echo peaks in region four. At $120kHz$, an interesting concentration of the regions where sandeels were found can be observed.

6.3.5 Slope of echo tail

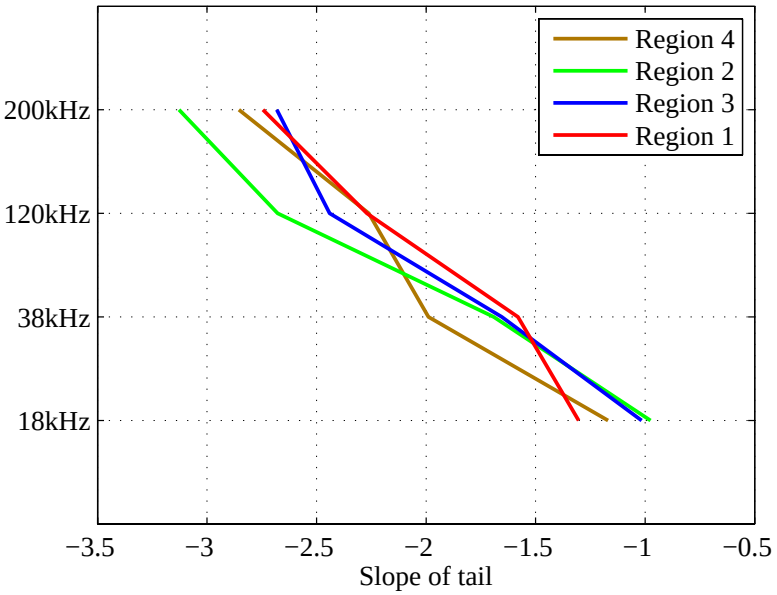

Figure 55: Slope of the echo tail for different frequencies, plotted for the different regions.

In figure 55, the calculated slopes for the different frequencies and for each of the sea floor regions are plotted. The reason for not plotting the standard deviation was to not deteriorate the visually closeness of the plots. It is however worth noting the variability was large between different variables of each of the regions.

When analyzing the plots, for the $200kHz$–channel, region two has a steeper slope than the other regions. This can indicate a more flat sea floor for region two. Previously, there has also been indications of a more flat sea floor in region four, but this information is not possible to extract from the plot of region four in the figure.

7 Future work

The natural direction to take this project further, is by doing a multi–variate discrimination analysis of the calculated results. This is a statistical approach where several variables are included in a study in order to see which one(s) contribute to the discrimination between groups. This analysis could give a more detailed picture of the differences between the calculated variables for different frequencies and regions of the sea floor, than the observation–based analyzation technique of this report. With the discrimination analysis, it should be possible after calibrating over a known bottom type, which could be a typical sandeel ground, to distinguish the echo variables that match the echo variables of this ground. Several tools and literature exist on the subject of discriminating analysis. Matlab for example, has its own multivariate statistics toolbox.

There is also possible to strengthen the variable analysis by calculating even more parameters of the echoes. QTC–View calculates for example 166 different parameters. However, this number of different parameters would probably not be very necessary or significant for a good analysis – the importance is what parameters that are calculated, not the amount. If still more echo parameters should be found for the classification, for eliminating redundant parameters, a principal component analysis that reduce multidimensional data sets to lower dimensions could be used.

In addition to the Sv values that were used for finding the variables in this project, there lies much information in the phase of the received echo. With a split–beam echosounder, as the echosounder provided the data for this project, the direction of the sources creating the echoes can be found within the beam. When the transmitted pulse reaches the sea floor a phase shift occur and this information can be used for estimating the bottom slopes with great precision. In this report only close to perfectly horizontal sea floors were studied, but when the bottom slope is known there also might be possible to evaluate sloping sea floors. Then, the sloping effects can be studied in more detail and possibly compensated for.

Future work should in addition support calculated echo variables by ground truth measurements. This task is also important for finding more exact parameters of typical sandeel grounds.

8 Conclusions

In this report a phenomenological characterization technique of received bottom echoes has been developed and studied, to evaluate the potential of locating typical sandeel grounds. Data from a calibrated multi–frequency echosounder operating at $18kHz$, $38kHz$, $120kHz$ and $200kHz$ were imported into Matlab with echosounder *.raw* data routines provided by Institute of Marine Research. First, the data were converted to Sv values where compensation for spherical spreading and absorption were utilized. Then the first received bottom echo was located in each ping and the threshold alignment method found suitable for aligning pings of each pingset, before averaging and smoothing were performed to reduce possible noise and ping to ping instabilities. Before further calculations, additional time correction was utilized to compensate for depth dependency between pingsets.

During the SMASSC 2008 survey, on board the vessel S/V Johan Hjort, both acoustic data and sandeel samples were collected in the sandeel fishing grounds of "Vestbanken" and "Elbow Spit North". From the Simrad SEABEC software a distinction could be made and different hardness and roughness properties found, between sea floor areas of large sandeel catch–sizes and distinctive SEABEC classification results of "Vestbanken". However, no conclusions could be made when results from "Elbow Spit North" was indistinct and the results from "Vestbanken" showed possible ambiguities.

To be able to establish possible characteristic features of bottom echoes from sandeel grounds, different parameters describing the bottom echo were calculated for sea floor regions with large sandeel catch–sizes during the SMASSC survey. These calculated parameters were compared together with parameters from regions where no sandeels were found. 30 consecutive pingsets were extracted from each region to determine the concentration of the calculated parameters. Especially the calculated total echo area showed an interesting frequency response for two of the regions of large sandeel catch–sizes. The shape of their frequency response were almost identical. However, the region with the second largest catch–size in "Vestbanken" differed and was more consistent with the region where no sandeels were found.

τ effective values have the potential of describing the main peak of the echo and could indicate variation in sediment scattering properties at lower frequencies. These values showed a trend at different frequencies for the different regions of the sea floor. The region of no sandeel catch–size had for all frequencies smallest τ values. This information could indicate less probability of a sandeel ground for such values, but because of possible ambiguities in the calculating routines of the τ values for high echo maximum peaks no conclusions can be made. The τ values can in addition together be seen as more detailed versions of the echo fall–time, when the rise–time stays the same for horizontal sea floors with small amount of fluctuations in relief heights.

A multi–variate analysis approach is the next step for this project. Many of the parameters analysed in this report have shown discriminating power and could after ground

truth measurements, cluster distinctive features of different seabed types. However, this report has shown an indication that sandeel grounds not are consistent between calculated seabed echo parameters. Besides, ambiguities as a result of echo fluctuations caused by both known and unknown sources could cause false estimates of echo parameters.

In addition, more tests of the calculation routines should be utilized. The Matlab routines can be used for calculating echo parameters after a survey when bottom depth and sampling frequency are known, but is far from having the possibility of real–time calculations at this state.

References

[1] Paul A. Clarke and L. J. Hamilton. The abcs program for the analysis of echo sounder returns for acoustic bottom classification. Technical report, Maritime Operations Dicision, Aeronautical and Maritime Resarch Laboratory, 1999.

[2] Christian de Moustier. Beyond bathymetry: Mapping acoustic backscattering from the deep seafloor with sea beam. Technical report, Marine Physical Laboratory, Scripps Institution of Oceanography, University of California, San Diego, California 92093, 1985.

[3] Herman H. Essen. Scattering from rough sedimental seafloor containing shear and layering. *Jour. Acoust. Soc. Am.*, 95(3):1299–1310, 1994.

[4] Jens M. Hovem. The physics of sound in underwater environments. Part 2, Chapter 12–18, 2007.

[5] Darrell R. Jackson, PKevin B. Briggs, Kevin L. Williams, and Michael D. Richardson. Tests of models for high–frequency seafloor backscatter. *IEEE Journal of Oceanic Engineering*, 21(4):458–470, 1996.

[6] Darrell R. Jackson and Pierre D. Mourad. High frequency sonar equation models for bottom backscatter and forward loss. *OCEANS'89. Proceedings*, 4:1168–1175, 1989.

[7] Darrell R. Jackson and Michael D. Richardson. *High–Frequency Seafloor Acoustics.* Springer New York, 2007.

[8] Darrell R. Jackson, Dale P. Winebrenner, and Akira Ishimaru. Application of the composite roughness model to high–frequency bottom backscattering. *Jour. Acoust. Soc. Am*, 79(5):1410–1416, 1986.

[9] Xavier Lurton. *An Introduction to Underwater Acoustics, Principles and Applications.* Praxis Publishing, 2002.

[10] J. A. Ogilvy. *Theory of Wave Scattering from Random Rough Surfaces.* IOP Publishing Ltd, 1991.

[11] Daniel D. Sternlicht and Christian P. de Moustier. Time–dependent seafloor acoustic backscatter (10–100 khz). *Jour. Acoust. Soc. Am.*, 114(5):2709, 2003.

[12] P.J. Wright, H. Jensen, and I. Tuck. The influence of sediment type on the distribution of the lesser sandeel, *ammodytes marinus*. *Jour. of Sea Research*, 44:243–256, 2000.

A Numerical approximation for the Kirchhoff backscattering cross section

$$\sigma(\theta) = \frac{bq_c|V_{ww}(90^{\cdot})|^2}{8\pi[\cos^4(\theta)^\alpha + aq_c^2\sin^4(\theta)]^{\frac{1+\alpha}{2\alpha}}}, \tag{41}$$

where the different constants a, b and q_c are given as

$$q_c = C_h^2 2^{1-2\alpha} k^{2(1-\alpha)}, \tag{42}$$

$$a = \left[\frac{8\alpha^2\Gamma(\frac{1}{2\alpha}+\frac{1}{2})}{\Gamma(\frac{1}{2})\Gamma(\frac{1}{\alpha})\Gamma(\frac{1}{2\alpha})}\right]^{2\alpha}, \tag{43}$$

$$b = \frac{a^{\frac{1}{2}+\frac{1}{2\alpha}}\Gamma(\frac{1}{\alpha})}{2\alpha}, \tag{44}$$

where Γ is the gamma function, C_h^2 and α are given from equation 22 and 23 on page 15, $V_{ww}(90°)$ is given in equation 9 on page 12 and k is the wave number in water.

B Transducer data sheets

SIMRAD

18 kHz split-beam transducer

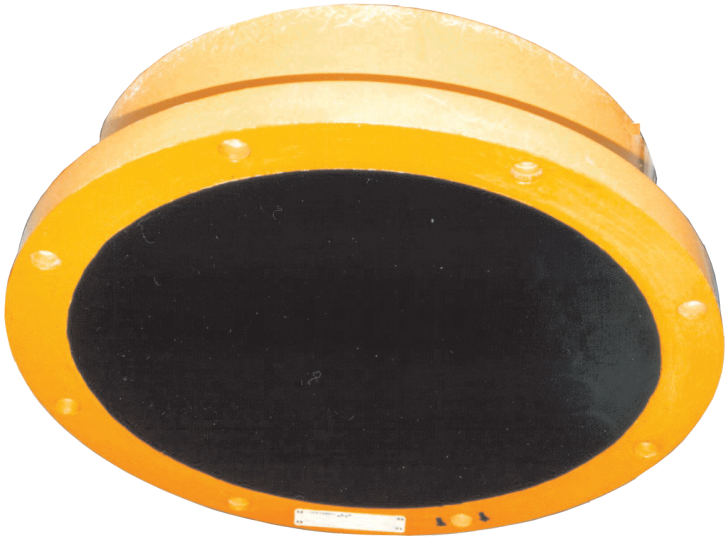

Introduction

The ES 18 is a split-beam transducer incorporating 44 tonpilz elements distributed over four quadrants. The following specifications are valid when all four quadrants are connected in parallel.

Order number

KSV-088694

Technical specifications

Resonant frequency ..... 18 kHz
Circular beamwidth ..... 11 ±2 deg
Directivity:
- D ..... 300 ±20 %
- DI=10 log D ..... 25 ±1 dB

Equivalent two-way beam angle:
- ψ ..... 0.020 ±20 %
- 10 log ψ ..... -17 ±1 dB

Side lobes ..... less than -18 dB
Back radiation ..... less than -35 dB

Impedance:
- Nominal value ..... 15 ohm
- Max. variation in |Z| ..... 11 to 20 ohm
- Max. variation phase angle ..... ±30 deg

Transmitting response ..... 182.0 ±2 dB (dB re 1µPa per V)
Receiving sensitivity, open circuit ..... -174 ±2 dB (dB re 1V per µPa)
Electroacoustic efficiency ..... 0.60 ±0.20
Maximum input pulse power ..... 2000 W
Maximum continuous input power ..... 100 W
Maximum transducer depth ..... 50 m
Cable length ..... 20 m
Cable diameter ..... 17.3 mm
Weight with cable ..... 85 kg
Storage temperature ..... +70 to -20 °C

(855-160506 Rev.C)

Data

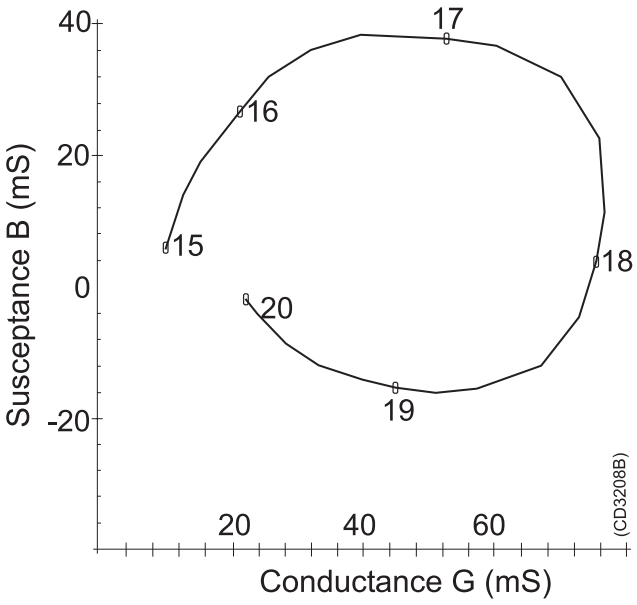

Admittance

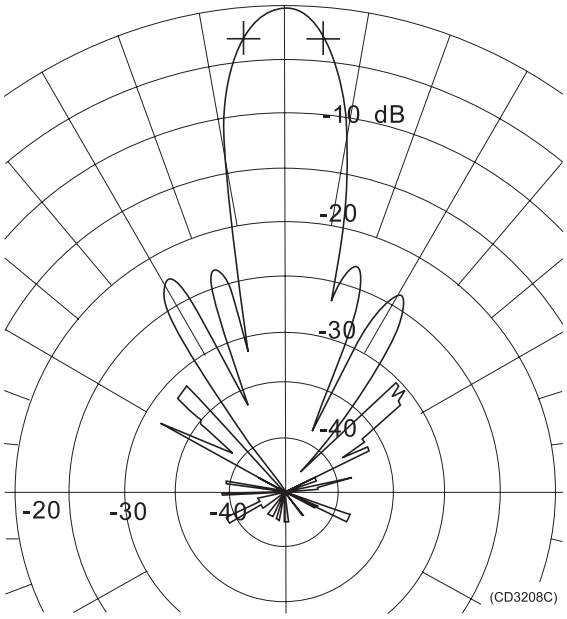

Beam pattern

Installation

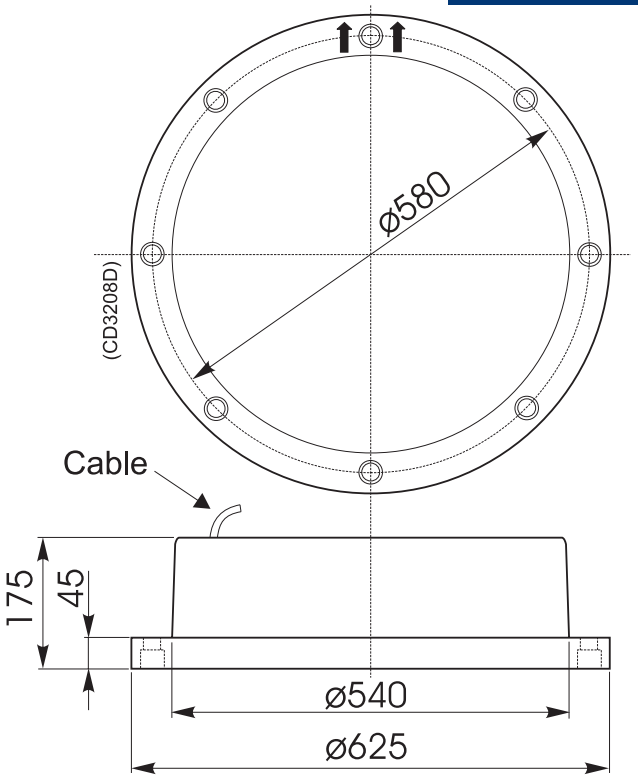

Outline dimensions

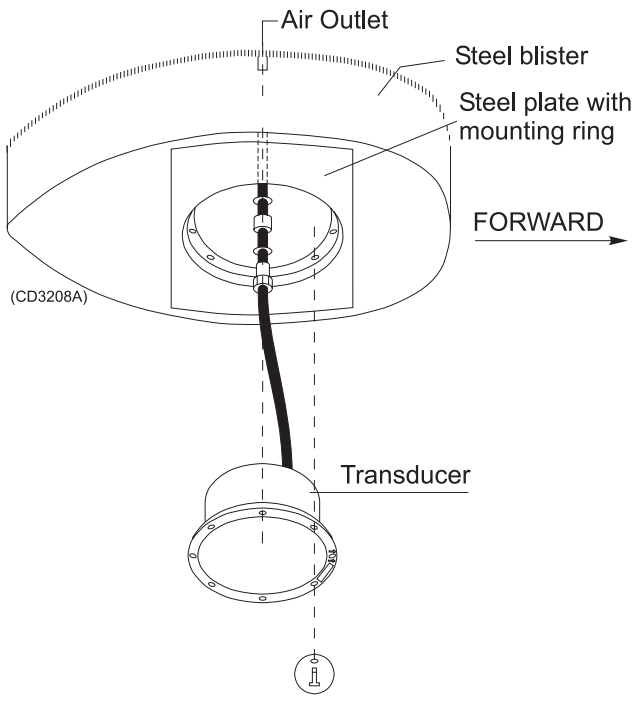

Installation example

Manufacturer:
Simrad AS
Strandpromenaden 50
P.O.Box 111
N-3191 Horten
Telephone: +47 33 03 40 00
Telefax: +47 33 04 29 87
Internet: www.simrad.com

38 kHz high power split-beam transducer

Introduction

The ES 38B is a split-beam transducer incorporating 88 piezo-ceramic elements distributed over four quadrants. The following specifications are provided with regard to all four quadrants connected in parallel.

Order number

KSV-074531

Technical specifications

Resonant frequency ..... 38 kHz
Longitudinal beamwidth ..... 7 ±1 deg
Transversal beamwidth ..... 7 ±1 deg
Directivity index ..... 28.0 ±1 dB
Equivalent two-way beam angle ..... -20.5 ±1 dB
Side lobes ..... less than -15 dB
Back radiation ..... less than -35 dB
Impedance:
- Nominal value ..... 15 ohm
- Max. variation in |Z| ..... 11 to 20 ohm
- Max. variation in phase ..... ±30 deg

Transmitting response ..... 185.5 ±2 dB (dB re 1µPa per V)

Receiving sensitivity:
- Open circuit ..... -176.5 ±2 dB (dB re 1V per µPa)

Electroacoustic efficiency:
- Typical ..... 70 %
- Minimum ..... 50 %

Maximum input power ..... 4000 W
Maximum duty cycle at max power ..... 1 %
Maximum transducer depth ..... 50 m
Cable length ..... 20 m
Cable diameter ..... 18 mm
Weight (without cable) ..... 40 kg
Storage temperature ..... +70 to -40° C

(855-164247 Rev.C)

Data

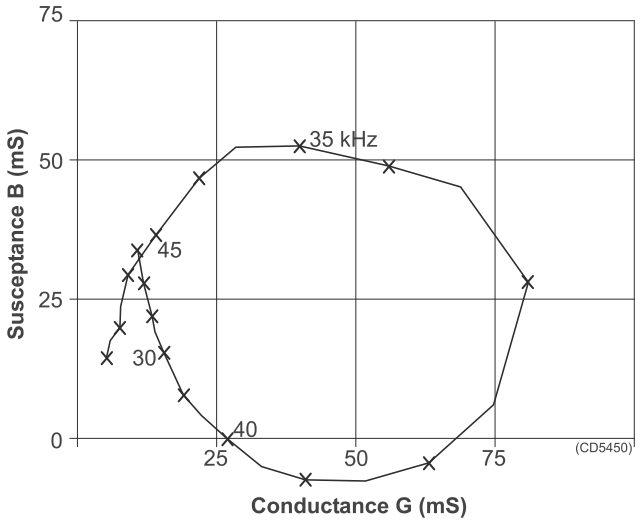

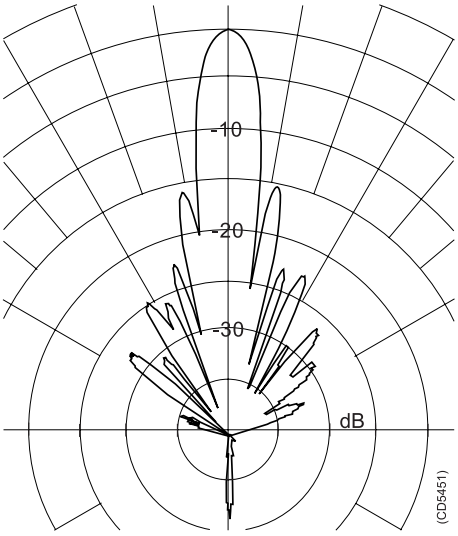

Installation

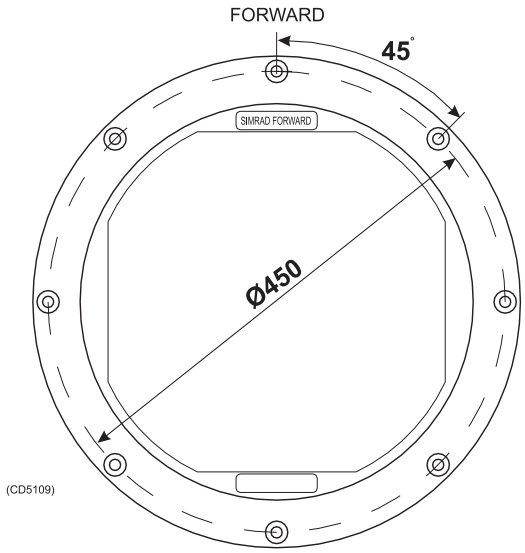

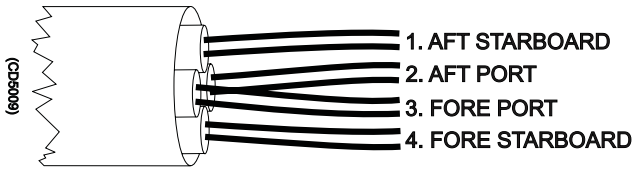

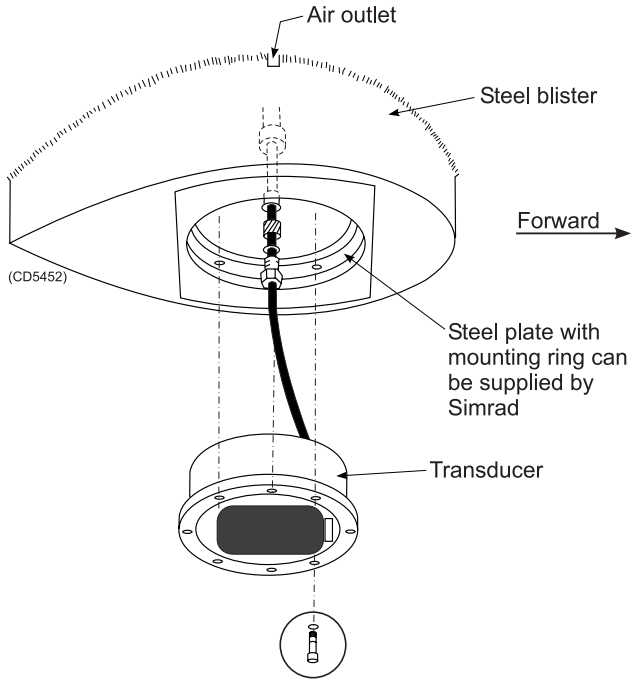

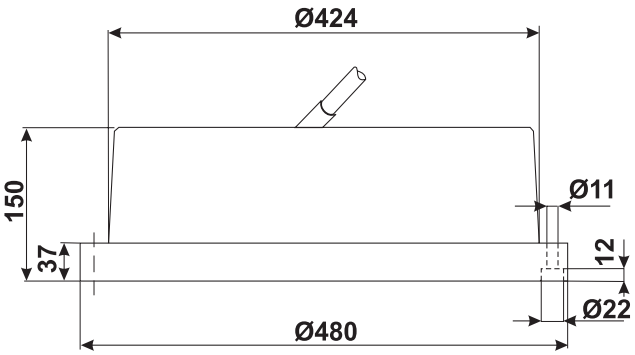

Manufacturer:
Simrad AS
Strandpromenaden 50
P.O.Box 111
N-3191 Horten
Telephone: +47 33 03 40 00
Telefax: +47 33 04 29 87
Internet: www.simrad.com

TRANSDUCER
Simrad ES 120-7

SIMRAD

120 kHz Split-beam transducer

Introduction
The ES 120-7 is a split-beam transducer with 76 piezo-ceramic elements arranged in four quadrants. The following specifications are valid when all four quadrants are connected in parallel.

Order number
KSV-088277

Technical specifications
Resonant frequency ..... 120 kHz
Beamwidth, circular ..... 7 deg ±1
Directivity:
- D ..... 650 ±20%
- DI=10logD ..... 28 ±1 dB

Equivalent two-way beam angle:
- Ψ ..... 0.009 ± 20% steradain
- 10 logΨ ..... -20.5 ±1 dB

Side lobes ..... less than -15 dB
Back radiation ..... less than -35 dB
Angle sensitivity:
- Phase angle/angle to target 21

Impedance:
- Nominal ..... 15 ohms
- Max. variation in |Z| ..... 11 - 20 ohms

Max variation in phase angle ..... ±30 deg
Transmitting response ..... 185.5 dB ±2 re 1µPa per V
Receiving sensitivity, open circuit ..... -186.5 dB ±2 re 1V per µPa
Electroacoustic efficiency ..... 0.70 ±0.20
Maximum pulse power input ..... 1000 W
Maximum continous power input ..... 10 W
Maximum transducer depth ..... 150 m
Cable length ..... 20 m
Cable diameter ..... 18 mm
Weight without cable ..... 5 kg
Storage temperature ..... -20 to 70 °C

(855-130262 Rev.C)

Data

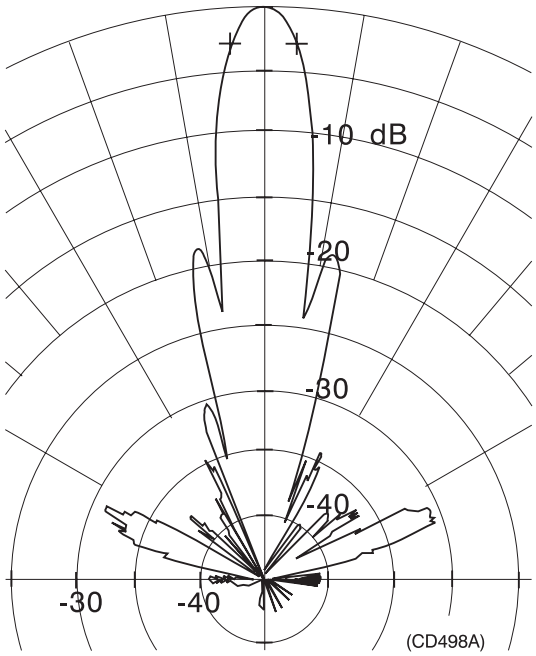

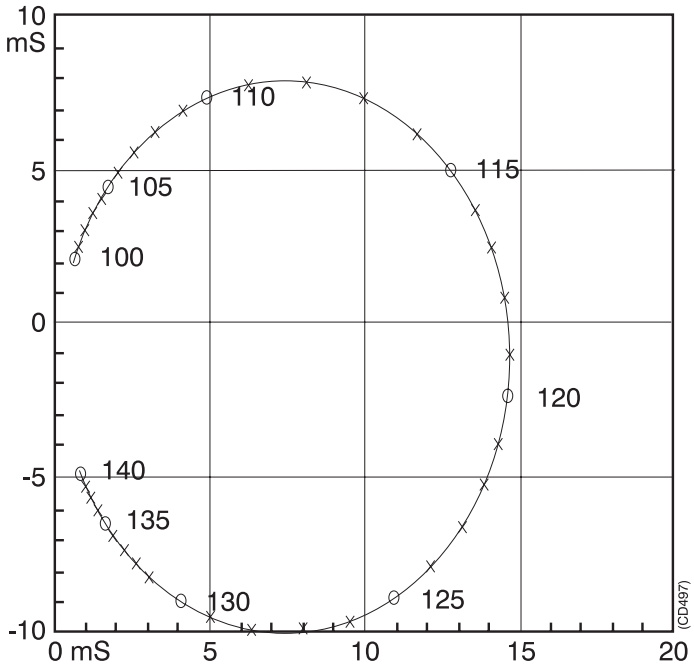

Installation

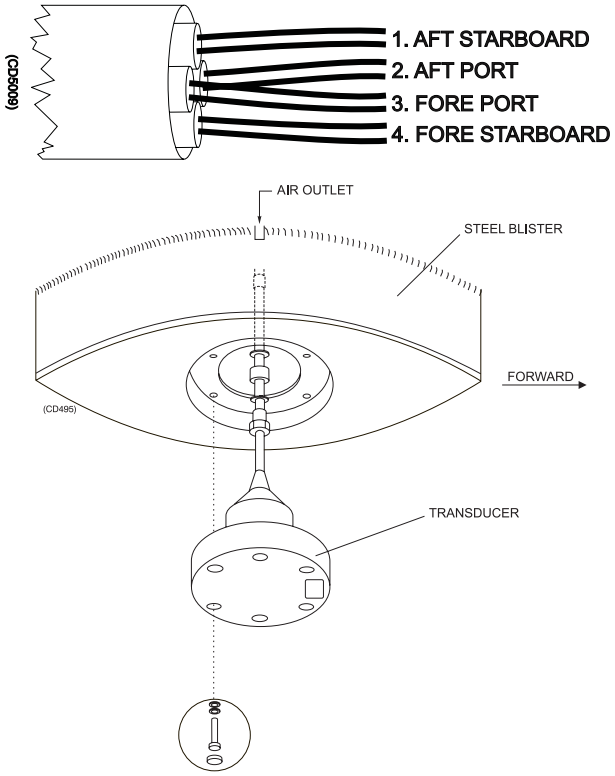

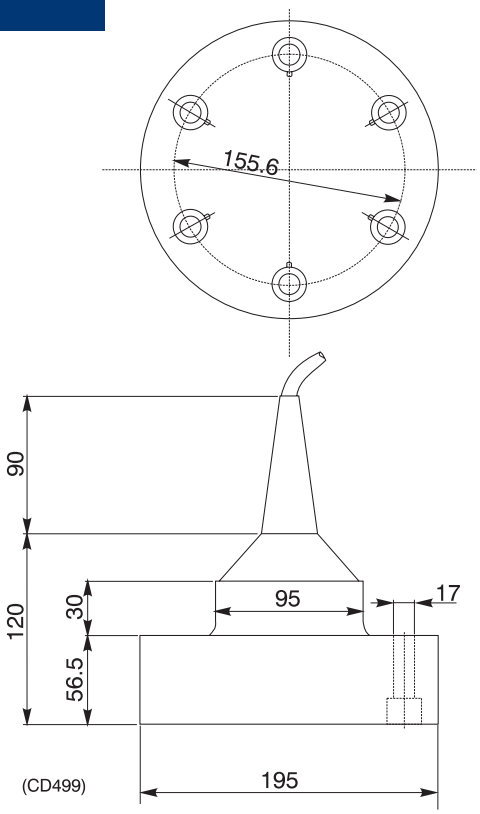

Manufacturer:

Simrad AS

Strandpromenaden 50

P.O.Box 111

N-3191 Horten

Telephone: +47 33 03 40 00

SIMRAD

Simrad ES 200-7
Transducer

Introduction

The ES 200-7 is a split-beam, composite transducer with a large bandwidth. This provides a fine range resolution, which is important for single fish detection and target strength measurement. The transducer has four quadrants. The specifications below are valid when all four quadrants are connected in parallel.

Order number

KSV-202718

Technical specification

Resonant frequency ..... 200 kHz
Beamwidth, circular ..... 7 ±1 deg
Directivity:
- D ..... 650 ±20 %
- DI=10 log D ..... 28 ±1 dB

Equivalent two-way beam angle:
- ψ ..... .0.009 ±20 %
- 10 log ψ ..... -21 ±1 dB

Side lobes ..... less than -23 dB
Back radiation ..... less than - 40 dB
Angle sensitivity 23
Impedance:
- Nominal ..... 19 ohm
- Maximum variation in | Z | ..... 15 to 24 ohm
- Maximum variation phase angle ..... ±30 deg

Transmitting response ..... 184 ±2 dB (re 1µPa per V)
Receiving sensitivity open circuit ..... -191 ±2 dB (re 1V per µPa)
Electroacoustic efficiency ..... 0.60 ±0.20
Maximum pulse power input ..... 1500 W
Maximum continuous power input ..... 10 W
Maximum transducer depth ..... 20 m
Cable length ..... 20 m
Cable diameter ..... 17.3 (+0.6, -0.2) mm
Weight without cable ..... 3 kg
Storage temperature ..... -20º to 70º C

(855-164298A / AA000 / 7-21)

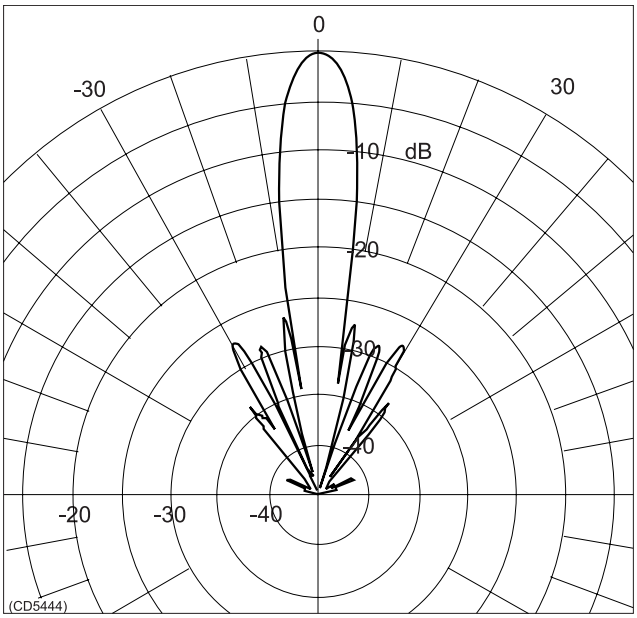

Beam pattern

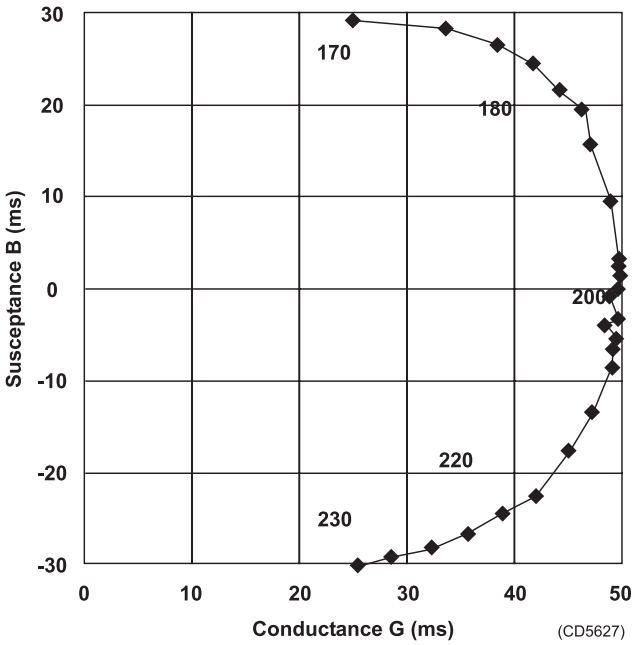

Admittance

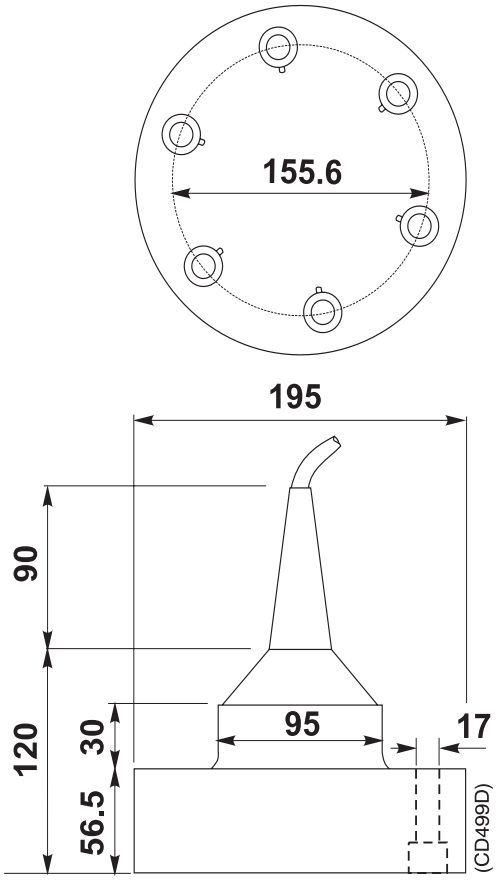

Outline dimensions

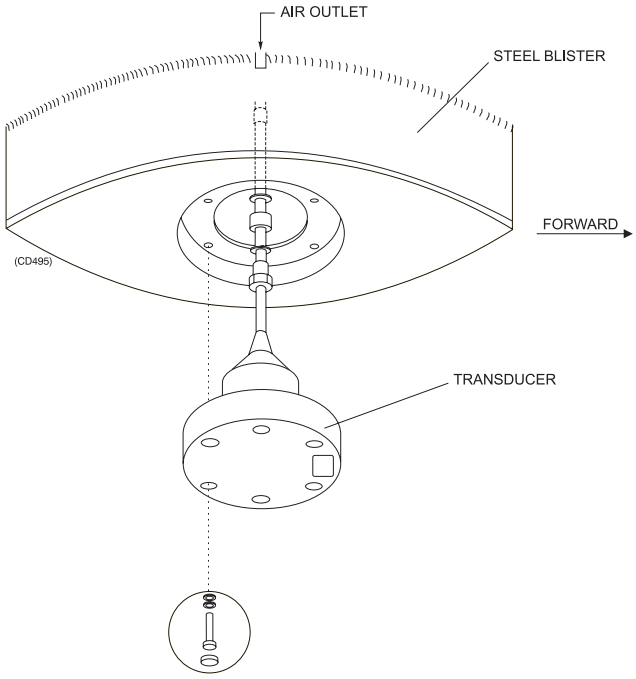

Installation example

Manufacturer:

Simrad AS
Strandpromenaden 50
P.O.Box 111
N-3191 Horten
Norway
Telephone: +47 33 03 40 00
Telefax: +47 33 04 29 87
Internet: www.simrad.com
E-mail: fish_research@simrad.com
fish@simrad.com